Fundamentals of optics and radiometry for color reproduction

Mathieu Hébert

Institut d'Optique, 42000 Saint-Etienne, France ; and Université de Lyon, Université Jean Monnet de Saint-Etienne, CNRS UMR 5516 Laboratoire Hubert Curien, 42000 Saint-Etienne, France

Roger D. Hersch

Ecole Polytechnique Fédérale de Lausanne (EPFL), School of Computer and Communication Sciences, 1015 Lausanne, Switzerland.

Patrick Emmel

Clariant International Ltd., Rothausstrasse 61, 4132 Muttenz, Switzerland.

ABSTRACT

Visual appearance of objects comes from the interpretation by the human visual system of a light signal issued from the objects. Describing or predicting appearance is therefore a question of light and requires notions about light propagation and measurement. In this paper, we introduce basic laws of optics, the science of light, and radiometry, the science of light measurement, in the context of colored surfaces. We address light spectrum and illuminants, polarization, notions of reflectance and transmittance based on radiometric definitions, gloss, absorption, scattering, fluorescence and models for light reflection and transmission by flat and rough surfaces, by slabs of nonscattering media and diffusing layers. Throughout the paper, we present the most current methods to assess the different physical quantities by measurement.

Key words

Optics, Radiometry, Reflectance, Transmittance, BRDF, Polarization, Illuminants, Refractive index, Reflection, Refraction, Fresnel's formulas, Scattering, Kubelka-Munk model, Gloss, Spectral measurement, Fluorescence.

1. INTRODUCTION

Coloring a surface to form an image is a very ancient activity which is based on a simple principle: the deposition of coloring layers on a reflecting support. In painting or analog photography, these coloring layers are continuous. They cover the entire surface and more or less absorb light depending on their thickness and dye concentration. The obtained colors are called 'continuous tone' or 'contone'. In printing, the coloring layers are discontinuous. The inks have

1

fixed thickness and colorant concentration; the different tones are obtained by varying their surface coverage ratio yielding the 'halftones' colors. Historically, the color rendering of images was controlled by the painter, the photographer or the printer, i.e. by a specialist who somehow acquired his expertise in the selection of the materials and the control of the coloration process. The new printing technologies have increased the image reproduction quality and the ubiquity of color images in everyday's life. They have also provided the possibility for non-expert consumers to print themselves at home thanks to fully automated printing processes. In the absence of a color expert, the printer needs to be calibrated by the constructor. This requires to relate color rendering to technical parameters (dye concentration, ink thickness, etc.) according to a scientific approach relying on physical measurements. The task of scientists in this domain is double: understanding the physical phenomena being at the origin of the color rendering, and predicting the color rendering for given printing specifications. These two topics are the subject of the following papers.

Before entering into the physical characterization of the printed colors, it should be recalled that color is not a physical quantity but a physiological sensation. This sensation is the response of our visual system to a light signal striking the retina. During the 20th Century, scientists managed to elaborate a mathematical description of the color sensation, and to connect it with the spectrum of the light received by the retina. However, the study of color and the study of light are two scientific domains based on very different concepts, called respectively colorimetry and optics. Light can be characterized by its energy, its speed, its wavelength, its direction, its polarization, but it would be erroneous to say that it "has a color". Likewise, it is simplistic to say that a surface "has a color". We should rather say that it has the aptitude to reflect a fraction of the ambient light depending on its spectrum attenuation capacities, which creates a luminous signal that human brain perceives as a color. A complete description of the print color rendering should therefore rely on physical as well as perceptual analysis. However, we generally assume that these two analyses can be treated separately, i.e. the luminous signal issued from the surface is fully characterized by the physics, and the interpretation of this luminous signal in terms of color is described by colorimetry. In this paper, we will focus on the physical analysis.

Optics is the scientific study of light and its interaction with matter. It covers a wide range of phenomena and applications. We focus here on the basic notions necessary to understand surface color prediction models. We first recall briefly what is light and what kind of light is considered in color reproduction. Then, we introduce radiometry, the branch of optics that deals with light measurement, as well as models for absorption, reflection and refraction by a surface, scattering and special effects like fluorescence.

2. LIGHT

According to the Commission Internationale de l'Eclairage (CIE), light is the generic name for the electromagnetic radiations visible to the human eye [1]. As every electromagnetic radiation, it can be considered as a wave phenomenon as well as a collection of particles called *photons*, propagating at a speed $c \approx 2.998 \times 10^8$ m.s^{-1} in vacuum [2]. The simplest emission mechanism of light is due to isolated atoms which emit a photon when transiting from a high energy level to a lower energy level. Since the energy of atoms is quantized, only a finite number of possible energies can be given to the emitted photon. To each photon energy there corresponds a monochromatic wave characterized by its oscillation frequency ν or its wavelength $\lambda = c / \nu$. The vibration frequency is proportional to the photon energy *e* according to the relation $e = h\nu$, where $h \approx 6.626 \times 10^{-34}$ J.s is the Planck constant. The sensibility of the human eye to light is significant for wavelengths between 400 and 700 nanometers (nm), with a maximum around 555 nm (photopic vision) or around 501 nanometers in dark context (scotopic vision). However, the notion of light can be extended to infrared (IR) and ultraviolet (UV) radiations, having respectively longer and shorter wavelengths but similar physical properties.

2.1. Wave optics and polarization

According to the wave model, light is composed of an electric field and a magnetic field oscillating in phase, perpendicular to each other and both perpendicular to the propagation direction. The two fields are modeled as three-dimensional vectors, respectively **E** and **B**, being functions of time and position. Maxwell's equations describe their variation in time and space according to the electrical properties of the propagation medium. When the medium is not vacuum, the propagation speed *v* is slower than *c*. The ratio *c/v*, called *refractive index*, characterizes the optical properties of the medium.

The electric and magnetic fields oscillate in the plane orthogonal to the propagation direction. *Polarization* denotes the time-dependent orientation of the electric field **E** (thereby of the magnetic field which is perpendicular to it) in this plane [3]. A convenient way to describe polarization is to project vector **E** on two orthogonal axes of the plane. One obtains two components E_x and E_y being periodical functions of time with identical period, whose phase difference indicates the polarization. If E_x and E_y oscillate in phase, **E** oscillates according to a straight line and polarization is said to be *linear* (see Figure 1). If the phase difference between E_x and E_y is $\pm \pi / 2$, **E** draws a circle and polarization is said to be *circular*. *Elliptic* polarization corresponds to the other phase differences. Polarization is generally modified when light interacts with matter, for example when it is reflected or refracted at the interface between media with different refractive indices.
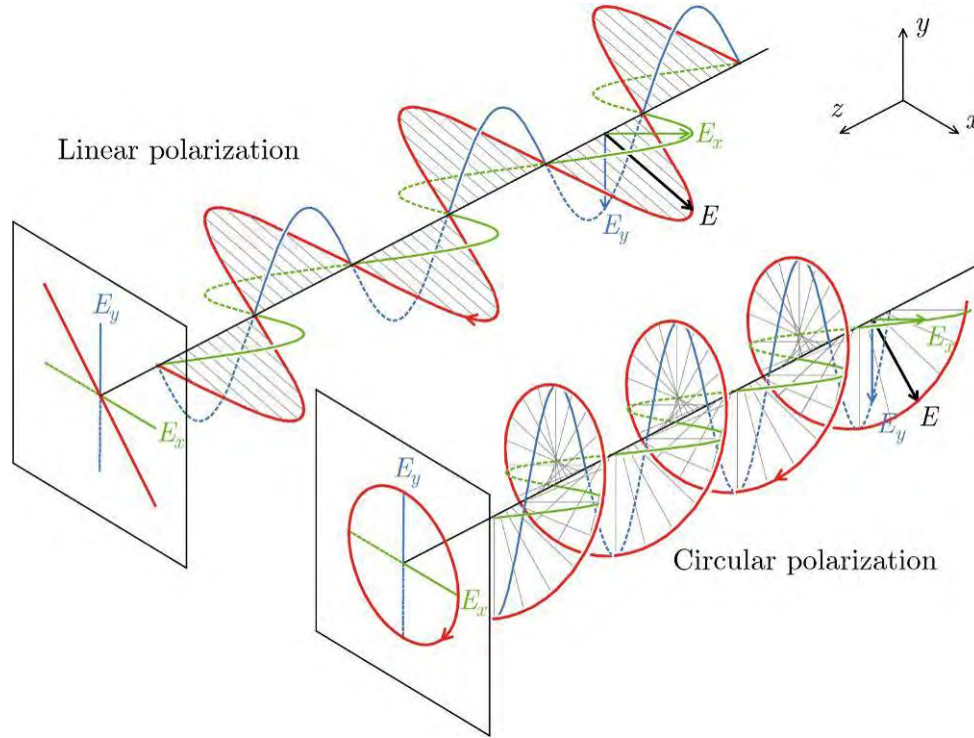
Figure 1. Propagation of the electric field for linear and circular polarizations of light.

2.2. Natural light

The light emitted by the sun and most common light sources is composed of many short wave packets independent of each other and having different polarizations. Polarization therefore varies rapidly in a random and irregular manner. Such light is called *natural light*. It is modelled as the sum of two linearly polarized lights independent of each other, whose respective electric fields oscillate in perpendicular directions. These two polarized lights are generally denoted by the symbols *p* and *s*, whose meaning will appear clearly in Section 4.2. Their respective powers Φ_p and Φ_s determine the *degree of polarization* (DOP) defined as [4,5]

$$DOP = \frac{\max\left(\Phi_p, \Phi_s\right) - \min\left(\Phi_p, \Phi_s\right)}{\max\left(\Phi_p, \Phi_s\right) + \min\left(\Phi_p, \Phi_s\right)} \tag{1}$$

The DOP is 0 when the two components have equal power and 1 when one of the two components is zero, which corresponds respectively to *unpolarized* and *totally polarized natural light*. A DOP value between 0 and 1 indicates that the light is *partially polarized*.

2.3. Light ray and geometrical optics

The light ray concept is evident for everyone. It comes from the observation that light propagates along straight lines in homogenous media, e.g. air or clear water. However, it has no physical existence. It is only an approximated model describing the propagation of light when its wave property can be ignored. In practice, the ray concept is sufficient to describe reflections and

4

refractions as well as the trajectory of light beams through optical systems, provided the large distance compared to the wavelength separates successive variations of refractive index. Light rays are the basis of a domain of optics called g*eometrical optics*.

Light rays are independent of each other. This means that there is no *spatial coherence* between them. When two rays are superposed, their energies are simply added without any interference or diffraction phenomenon. According to Huygens' principle [37], the condition for this independence property is that the cross section of the ray (also called *extent*) is much larger than the wavelength. The principle of Fermat, also known as the *least time principle*, asserts that light follows the quickest optical path between two given points. In a medium of constant refractive index, light propagates at constant speed and the quickest path is a straight line. If the refractive index varies, the quickest path may follow a bended or curved line. The set of points being at the same optical length from a point source is called the *wave surface*. *Malus' law* asserts that the wave surface is always perpendicular to the ray, even after various reflection or refraction events [37]. In a light pencil, the optical length between two wave surfaces is the same for all rays.

2.4. Interaction between light and colored surfaces

The materials used in printing, i.e. papers, plastics and inks, have very complex structures. The refractive index of the materials, which determines how light propagates in them, varies locally in an irregular manner. The paper fibers and the ink pigments provoke multiple diffraction events which would be impossible to describe all rigorously. However, since heterogeneities are randomly distributed in the media, these diffraction events yield no perceptible colored effect. They simply contribute to a global light diffusion process. Instead of describing the complex, random paths followed by waves in the colored materials, one rather considers average photon transfers such as the transfer from a source to a detector or the transfer from one layer to another. This assumption considerably simplifies light-print interaction models and allows staying in the geometrical optics domain. The measurement of these light quantities and the study of their distribution in space are the aim of radiometry.

3. RADIOMETRY

Radiometry is the science of the measurement of radiations. It comprises the study of radiation emission by sources, detection, reflection or transmission through optical systems, etc. It thus gives rise to a profuse literature (*see* for example references [5, 6, 7, 8, 9, 10, 11, 12]). Radiometry differs from optics in the sense that it focuses on energy measurement, without having to consider specifically any type of material. However, it is crucial to know the properties of light to perform appropriate measurements and interpret them correctly. Most of the radiometry is based on incoherent radiations and on the geometrical optics of rays. Most of the time, wave phenomena such as diffraction and interferences are ignored. Radiations are measured in terms of absolute

power and the measurements are expressed in energy units. The considered type of radiation depends on the source and the detector. The perception of light by a human observer is studied in a separate discipline called *photometry*. The radiant power at each wavelength is weighted by a visual sensitivity function that models human brightness sensitivity. The measured quantities are expressed in *luminous units* called lumen, candela and lux, especially used for the characterization of light sources. The distinction between optical radiometry and photometry is linked to the history of radiation measurement, but they use similar concepts and are almost synonymous today.

The interest of radiometry in appearance assessment is the possibility to quantify the amounts of light being in interaction with the object and their transfer from a source to a detector. The fundamental radiometric quantities describe the geometrical distribution of energy in space and the reflection or transmission properties of objects can be defined as ratios of them, called accordingly *reflectance* or *transmittance*. In this section, we introduce the radiometric definitions leading to the reflectance and transmittance concepts and address the main tools for their measurement.

3.1. Geometrical concepts

Describing the transport of light from a source to an object, then from the object to an observer is first a question of geometry. If one defines a light ray as the photons passing through two points P_1 and P_2, the ray would contain no photon because the probability for a photon to meet precisely one point or to follow one direction is zero. One should rather consider a small area around each point and a small set of directions. The set of directions is called *solid angle*, and its coupling with a small area is called *geometrical extent*.
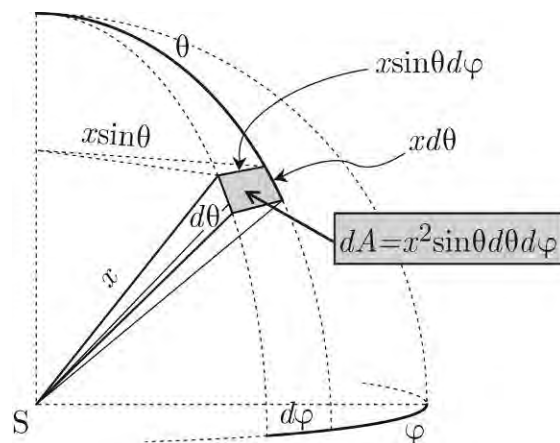
Figure 2. Differential solid angle in the direction (θ,φ).

An infinitesimally small solid angle points at one direction which is generally specified by its polar and azimuth angles (θ, φ) in spherical coordinates. Figure 2 shows that it intercepts an area $x^2 \sin \theta d\theta d\varphi$ on the sphere of radius x. The infinitesimal solid angle is therefore

$$d\omega = \sin \theta d\theta d\varphi \tag{2}$$

The *geometrical extent* denotes the geometry of a light pencil propagating between two small surface elements, ds_1 and ds_2 (Figure 3). By assuming that the distance x between them is sufficiently large, one may consider that the rays received by ds_2 come from one point P_1 on ds_1. Similarly, one may consider that the rays emitted by ds_1 reach one point P_2 on ds_2. The line (P_1P_2) gives the direction of the light ray. It forms an angle θ_1 with the normal of ds_1 and an angle θ_2 with the normal of ds_2. The solid angle based in P_1 subtended by ds_2 intercepts an area dA_2 on the sphere of radius x centered in P_1. It is therefore

$$d\omega_1 = dA_2 / x^2 = ds_2 \cos \theta_2 / x^2 \tag{3}$$

Likewise, the solid angle based in P_2 subtended by ds_1 is

$$d\omega_2 = dA_1 / x^2 = ds_1 \cos \theta_1 / x^2 \tag{4}$$

The geometrical extent of the light pencil [5], expressed in $m^2.sr$, is defined as

$$d^2G = dA_1 d\omega_1 = dA_2 d\omega_2 = \frac{dA_1 dA_2}{x^2} = \frac{1}{x^2}\left(ds_1 \cos \theta_1\right)\left(ds_2 \cos \theta_2\right) \tag{5}$$
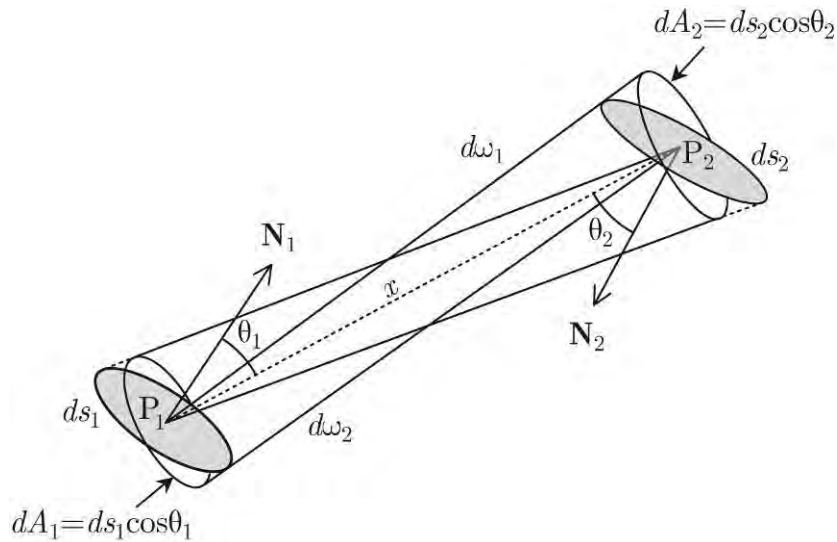

Figure 3. Elementary pencil of light between two small surface elements ds_1 and ds_2.

3.2. Radiometric quantities

Radiometric rules are based on four fundamental quantities: radiant flux, radiant intensity, irradiance and radiance. *Radiant flux* Φ (or simply *flux*) is the energy radiated per unit time expressed in watts (W).

Radiant intensity I is the density of flux per unit solid angle that is emerging from a point in space and propagating in a specified direction $d\omega$ (expressed in W.sr^{-1})

$$I = \frac{d\Phi}{d\omega} \tag{6}$$

Intensity is rather used for point sources that cannot be given a well defined area, such as stars in astronomy.

Irradiance E is the density of flux per unit area that is incident on a specified point in a specified surface, expressed in W.m^{-2}. If one considers a flux $d\Phi$ relatively to a surface element *ds*, the corresponding irradiance is

$$E = \frac{d\Phi}{ds} \tag{7}$$

Irradiance is a function of position on the surface. *Exitance M* is the equivalent of irradiance when light emerges from the surface instead of being incident.

Radiance L is the flux per unit extent that is incident on, passing through or emerging from a specified point in a specified surface in a specified direction, in W. m^{-2}.sr^{-1}

$$L = \frac{d^2\Phi}{d^2G} \tag{8}$$

Radiance is the most suitable radiometric quantity to describe thin light pencils. Its relationship with the geometrical extent provides interesting geometrical properties: if we consider a flux propagating between two small surface elements, we can be certain that the radiance emitted by the one is equal to the radiance received by the other one. This principle, called the *radiance invariance*, is a direct consequence of equation (5). If one considers a surface element *ds* and a differential solid angle $d\omega = \sin\theta d\theta d\varphi$ oriented at θ to the normal of *ds*, the differential extent is $dG = ds\cos\theta d\omega$. The radiance is thus expressed as

$$L(\theta,\varphi) = \frac{d^2\Phi}{ds\cos\theta d\omega} \tag{9}$$

In equation (9), the ratio $d^2\Phi/ds$ corresponds to the elemental irradiance *dE* attached to the light pencil. It is related to the radiance by

$$dE(\theta,\varphi) = L(\theta,\varphi)\cos\theta d\omega \tag{10}$$

3.3. Photometric units

Photometry differs from radiometry by the fact the energy is weighted by the spectral sensibility of the human eye [14], usually denoted as $V(\lambda)$, plotted in Figure 4.
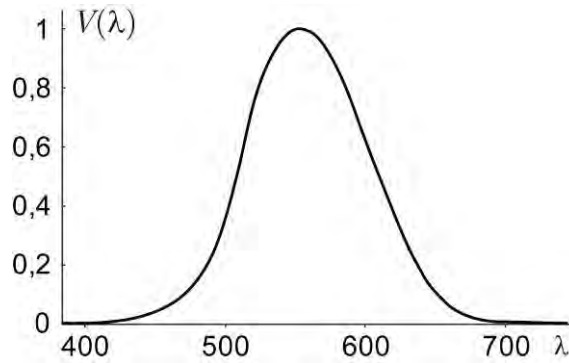
Figure 4. Spectral sensitivity of the human eye in photopic vision.

The flux is called *luminous flux* and is expressed in lumen (lm). The equivalent for irradiance is *illuminance* in the case of an illuminated surfaces or *luminous exitance* in the case of an emitting surface (expressed in lux). The *luminous intensity* is expressed in candela (cd) and the radiance, called *luminance*, is expressed in candela per square meter ($cd.m^{-2}$).

3.4. Lambert's law

Although the notion of diffuse light is intuitive, it can be given a rigorous meaning thanks to the radiance concept. According to Lambert's law, a perfectly diffusing surface emits or reflects the same radiance in every direction. It is thus called a *Lambertian surface* or *reflector.*

According to relation (10), the elemental exitance issued from the surface in some direction (θ, φ) is

$$dM(\theta, \varphi) = L \cos \theta \, d\omega \tag{11}$$

where $d\omega = \sin \theta d\theta d\varphi$ is the infinitesimal solid angle and L is a constant. By summing up the elemental exitance elements over the hemisphere, one obtains the following relation between radiance L and total exitance M:

$$M = \int_{\varphi=0}^{2\pi} \int_{\theta=0}^{\pi/2} L \cos \theta \sin \theta \, d\theta d\varphi = \pi L \tag{12}$$

In practice, many sources are Lambertian and strongly scattering materials such as paper bulk, cotton furniture or milk are Lambertian reflectors.

3.5. Bi-directional Reflectance Distribution Function

According to Nicodemus [17], the reflection process of light by a surface is embodied in the fundamental equation relating the elemental irradiance dE_i coming from each direction (θ_i, φ_i) and the radiance $dL_r(\theta_r, \varphi_r)$ reflected into each direction (θ_r, φ_r)

$$dL_r(\theta_r, \varphi_r) = f_R(\theta_i, \varphi_i; \theta_r, \varphi_r) dE_i(\theta_i, \varphi_i) \tag{13}$$

Function f_R is called *bidirectional reflectance distribution function* (BRDF). Thanks to the relation (10), it can be defined in terms of the incident radiance $L_i(\theta_i, \varphi_i)$:

$$dL_r(\theta_r, \varphi_r) = f_R(\theta_i, \varphi_i; \theta_r, \varphi_r) L_i(\theta_i, \varphi_i) \cos\theta_i d\omega_i \tag{14}$$

In the case of a nonabsorbing Lambertian reflector, the total outgoing exitance E_r is equal to the incident irradiance. Since the reflected radiance is E_r/π in every direction, the BRDF is a constant equal to $1/\pi$. Thus, the spectral BRDF depends only on wavelength and is easier to measure. In the case of a perfect mirror, the BRDF cannot be defined. A setup for mirror reflectance measurement is described in Ref. [18, p. 54]. Figure 5 shows BRDF sections in the incidence plane of a Lambertian reflector, a smooth surface, roughened aluminium surface [19] and a glossy paint.

BRDF is a function of many parameters: the four angles denoting the incidence and observation directions, and possibly wavelength of light, polarization, position on the surface… It is therefore impossible to plot a full BRDF on 2D graphic. 3D visualization by software is often preferred. However, planar mapping is good alternative for BRDF display [21].
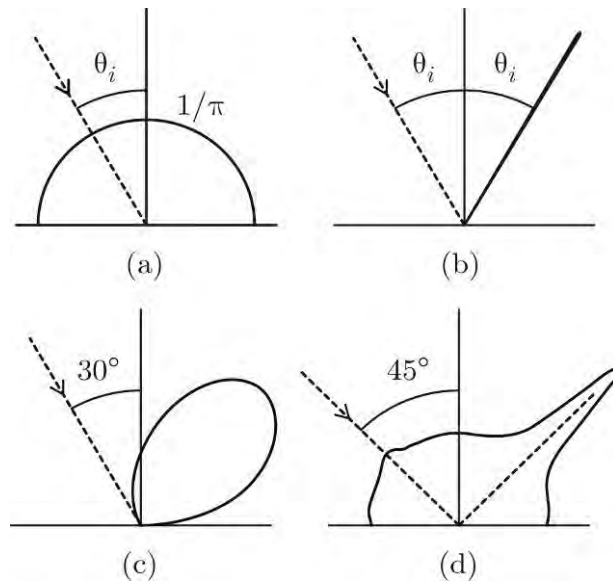

Figure 5. Sections of BRDF in the incidence plane ($\varphi_i = \varphi_r = 0$), plotted in polar coordinates as a function of θ_r, of (a) a Lambertian reflector, (b) a smooth surface, (c) a roughened aluminium surface and (d) a glossy paper [20].

The Lambert azimuthal equal-area projection [22] is especially convenient as it conserves areas: a portion of hemisphere with area A is mapped into a portion of disk with same area A. Every point P on the hemisphere of radius 1, specified by its spherical coordinates (θ, φ), is mapped to a point P' of polar coordinates (r, φ) contained within a disk of radius $\sqrt{2}$ tangent to the hemisphere at the North pole N (Figure 6).

The azimuth coordinate φ is the same in the two coordinate systems. Coordinate r corresponds the distance NP:
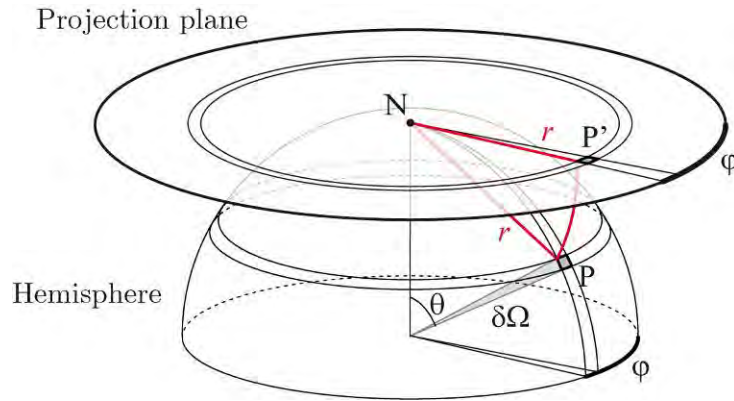
$$r = 2\sin(\theta/2)$$

Figure 6: Mapping of the hemisphere onto a disk of radius $\sqrt{2}$ according to Lambert azimuthal equal-area projection applied at the North pole N.

Point P' is also specified by the following Cartesian coordinates

$$u = 2\sin(\theta/2)\cos\varphi$$
$$v = 2\sin(\theta/2)\sin\varphi$$

(15)

Applying this mapping to the BRDF yields a multispectral image containing as many channels as wavelengths. Each pixel of the image corresponds to a same solid angle. Square pixels with size d represent solid angles of d^2 steradians.

Spectral BRDF is measured with a *gonio-spectrophotometer.* The incident light, generally brought by an optical fiber, is collimated with an optical system in such manner as to illuminate the sample with well parallel rays. In classical configurations, a rotating arm enables choosing the incidence direction. The reflected light is captured through a very thin solid angle by an optical system located on a second rotating arm. Light is then transferred to a spectrophotometer. Spectral measurements are performed at different detector positions. Although gonio-spectrophotometers can now be found at reasonable prices on the marketplace, their volume and fragility restrict their use for specific applications in laboratory.

3.6. Reflectance

The term *reflectance* denotes any ratio of reflected flux to incident flux being relative to a same surface element. Reflectance is therefore a ratio of exitance to irradiance. It is a dimensionless quantity depending on wavelength, direction, polarization and position on the surface. In this paper, we consider isotropic surfaces whose reflection properties are independent of position on average over areas of a few squared millimeters. We also consider natural light in the visible spectral domain. Thus, all radiometric quantities are spectral quantities defined for each of the two polarized components. However, as for the BRDF, dependence on wavelength and polarization are made implicit.

Many different reflectances can be defined in regard to the cone Γ_i through which light incomes and the cone Γ_r through which reflected light is observed. In the general case, the incident radiance $L_i(\theta_i, \varphi_i)$ is a function of direction (θ_i, φ_i) and creates, according to equation (10), the elemental irradiance $dE(\theta_i, \varphi_i) = L_i(\theta_i, \varphi_i)\cos\theta_i d\omega_i$. The total irradiance originating from Γ_i is given by the following integral:

$$E_{\Gamma_i} = \int_{(\theta_i, \varphi_i) \in \Gamma_i} L_i(\theta_i, \varphi_i)\cos\theta_i d\omega_i \tag{16}$$

The contribution of some incident radiance $L_i(\theta_i, \varphi_i)$ to one radiance $L_r(\theta_r, \varphi_r)$ is specified by the BRDF according to equation (14). The corresponding elemental exitance is

$$dM(\theta_i, \varphi_i; \theta_r, \varphi_r) = f_R(\theta_i, \varphi_i; \theta_r, \varphi_r)L_i(\theta_i, \varphi_i)\cos\theta_i d\omega_i \cos\theta_r d\omega_r \tag{17}$$

By summing up the contributions of all radiances contained within Γ_i, one obtains the elemental exitance in the direction (θ_r, φ_r)

$$dM(\Gamma_i; \theta_r, \varphi_r) = \int_{(\theta_i, \varphi_i) \in \Gamma_i} f_R(\theta_i, \varphi_i; \theta_r, \varphi_r)L_i(\theta_i, \varphi_i)\cos\theta_i d\omega_i \cos\theta_r d\omega_r \tag{18}$$

Then, by summing up all the elemental exitances through the observation solid angle Γ_r, one obtains the total exitance

$$M_{\Gamma_r} = \int_{(\theta_r, \varphi_r) \in \Gamma_r} \int_{(\theta_i, \varphi_i) \in \Gamma_i} f_R(\theta_i, \varphi_i; \theta_r, \varphi_r)L_i(\theta_i, \varphi_i)\cos\theta_i d\omega_i \cos\theta_r d\omega_r \tag{19}$$

The ratio of the exitance to the irradiance is the reflectance defined by the cones Γ_i and Γ_r, denoted as $R_{\Gamma_i : \Gamma_r}$

$$R_{\Gamma_i : \Gamma_r} = \frac{\int_{(\theta_r, \varphi_r) \in \Gamma_r} \int_{(\theta_i, \varphi_i) \in \Gamma_i} f_R(\theta_i, \varphi_i; \theta_r, \varphi_r)L_i(\theta_i, \varphi_i)\cos\theta_i d\omega_i \cos\theta_r d\omega_r}{\int_{(\theta_i, \varphi_i) \in \Gamma_i} L_i(\theta_i, \varphi_i)\cos\theta_i d\omega_i} \tag{20}$$

Judd [23] then Nicodemus [17] defined nine geometries where each of Γ_i and Γ_r is either directional, conical or hemispherical. By considering an isotropic reflector (BRDF independent of the incident azimuth angle φ_i) and a Lambertian illumination (constant radiance L_i), expression (20) noticeably simplifies. For example, the *directional-hemispherical reflectance* $R(\theta_i)$, or

simply "directional reflectance", is defined for directional illumination at (θ_i, φ_i) and a hemispherical observation:

$$R(\theta_i) = \int_{\varphi_r=0}^{2\pi} \int_{\theta_r=0}^{\pi/2} f_R(\theta_i; \theta_r, \varphi_r) \cos\theta_r \sin\theta_r d\theta_r d\varphi_r \qquad (21)$$

The *bi-hemispherical reflectance r*, or simply "Lambertian reflectance" is defined for Lambertian illumination through the hemisphere and hemispherical observation. It can be directly related to the directional reflectance [24]:

$$r = \int_{\theta_i=0}^{\pi/2} R(\theta_i) \sin 2\theta_i d\theta_i \qquad (22)$$

3.7. Reflectance factor

The reflectance measurement relies on two flux measurements: the reflected flux and the incident flux. As most instruments contain one detector which is used to capture the reflected flux, the incident flux cannot be measured directly. It is measured indirectly by using a perfect white diffuser able to reflect the incident light uniformly over the hemisphere without absorbing it. The flux captured by the detector is therefore proportional to the incident flux. The ideal white standard is a perfectly Lambertian, nonabsorbing and diffusing sample [26]. Its reflectance is equal to 1 and its BRDF is $1/\pi$ for every couple of incidence and reflection directions. In practice, white standards approaching these properties are made of pressed barium sulfate or PTFE (known as Algoflon, Halon or Spectralon). They must be calibrated in terms of the perfectly reflecting diffuser [27]. The object to assess and the perfect diffuser are illuminated and observed with the same geometry. The ratio $\hat{R}$ of the flux Φ measured from the object to the flux Φ_{ref} measured from the white diffuser is called *reflectance factor* [25]:

$$\hat{R} = \frac{\Phi}{\Phi_{ref}} \qquad (23)$$

A alternative definition is sometimes used when radiance measurements are performed: the ratio of radiance L measured from the object to radiance L_{ref} measured from the white diffuser is thus called *radiance factor* [18].

The reflectance and radiance factors are not rigorously reflectances. They coincide with reflectance in the case of Lambertian reflectors and provide a good approximation for matte papers and other nearly Lambertian reflectors. It is less relevant however for non-Lambertian reflectors such as glossy papers, mirrors or satine paintings. In some cases, the sample reflects more light towards the detector than the perfect diffuser and the reflectance factor overpasses one [28]. This occurs for example with a mirror illuminated by directional flux Φ_i at angle θ_i and observed by a radiance detector in the specular direction. The detector captures the flux $\Phi = R\Phi_i$ from the mirror, where R denotes the mirror's angular reflectance at the considered incidence, and

the flux $\Phi_{ref} = \Phi_i / \pi$ from the perfect diffuser. In this configuration, the reflectance factor of the mirror is higher than one at every wavelength where $R(\theta_i) > 1/\pi$.

3.8. Transmittance

All the definitions presented above regarding the reflectance of objects can be transposed to the transmittance. The equivalents for BRDF, reflectance and reflectance factor are respectively *BTDF* (*bi-directional transmittance distribution function*), *transmittance* and *transmittance factor*. This latter is defined in respect to the perfectly nonabsorbing transmitter, which in practice is air.

3.9. Spectral radiometry

The previous radiometric quantities have been defined without consideration of wavelength. The spectral distribution of the radiation is described by a *spectral flux* Φ_λ defined as flux per unit wavelength (in W.m^{-1}):

$$\Phi_\lambda = \frac{d\Phi}{d\lambda} \tag{24}$$

Spectral flux is measured with a spectrophotometer, generally in successive spectral bands. If the wavelength bandwidths $\Delta\lambda$ are small, the measured flux in each bandwidth is $\Phi_\lambda \Delta\lambda$. Over a larger band $[\lambda_1, \lambda_2]$, the measured flux is

$$\Phi_{[\lambda_1,\lambda_2]} = \int_{\lambda_1}^{\lambda_2} \Phi_\lambda d\lambda \tag{25}$$

The spectral resolution of spectrophotometers varies according to the application and the method used to decompose the light spectrum. For color reproduction applications, usual commercial instruments have a resolution comprised between 1 and 10 nanometers. In order to select narrow wavelength bandwidths, the light is decomposed according to a dispersing prism or a diffraction grating [13]. The location of the photodetector determines the measured wavelength domain. For faster measurements, the different wavelengths may be captured simultaneously by using an array of sensors (diode linear array, CCD linear array, etc.)

One similarly defines *spectral intensity* I_λ, *spectral irradiance* E_λ, *spectral radiance* L_λ.

The spectral reflectance is the ratio of reflected to incident spectral fluxes, both defined in the same small bandwidth $\Delta\lambda$ around the considered wavelength λ:

$$R(\lambda) = \frac{\Phi_{\lambda,r}\Delta\lambda}{\Phi_{\lambda,i}\Delta\lambda} \tag{26}$$

Spectral BRDF $f_r(\lambda)$, and *spectral reflectance factor* $\hat{R}_\lambda(\lambda)$, as well as *spectral BTDF* $f_t(\lambda)$, spectral transmittance $T(\lambda)$ and spectral transmittance factor $\hat{T}_\lambda(\lambda)$ are similarly defined. In the

following sections, all the radiometric quantities are spectral quantities but in order to simplify the notations, the term "spectral" and the index λ will be omitted.

3.10. Light sources and illuminants

The light source is a crucial element for the optical characterization of reflecting objects. Reliable characterization is possible only if the spectrum of the incoming light is non-zero for each wavelength band. The luminous power of the source should also be adapted to the sensitivity of the photosensor. A too weak flux at a given wavelength may decrease the signal-to-noise ratio of the detection system and induce a significant error in the measurement. Oppositely, a too strong flux saturates the photosensors. In the adequate power range, for each spectral band, one can assume that the reflected flux varies linearly with the incident flux (except in the special case of fluorescing objects which are treated in the last section of this paper). The ratio of these fluxes is therefore a constant, independent of the source power, which will be defined as being the *reflectance* of the object. However, although the source has no direct impact on optical properties of the object, its *spectral power distribution* (SPD) influences the perception of color. In colorimetry, relative SPD is called *illuminant*. Classical color spaces such as the CIELAB color space take it into account in the computation of the tri-chromatic coordinates of the colors. It is possible that two objects with different spectral reflectance $R_1(\lambda)$ and $R_2(\lambda)$ have the same color under the illuminant $I(\lambda)$ and different colors under the illuminant $J(\lambda)$, because the spectral radiances $R_1(\lambda)I(\lambda)$ and $R_2(\lambda)I(\lambda)$ correspond to *metameric* spectra whereas the spectral radiances $R_1(\lambda)J(\lambda)$ and $R_2(\lambda)J(\lambda)$ do not.

The ideal illuminant for reflectance measurement would be the *equal energy illuminant E* whose relative SPD is uniform over the visible spectrum. However, no natural or artificial lighting has a uniform SPD. In order to assess color rendering for most common lightings, the CIE defined various illuminants [14] inspired of the SPDs of incandescent light (illuminant A), of daylight (illuminants D) and of fluorescent lightings (illuminants F). Some of them are plotted in Figure 7. The relative SPD of illuminant A is issued from the spectral radiance of a black body at the temperature $T_A = 2848$ K given by Planck's law, normalized to the value 100 at the wavelength $\lambda_0 = 560$ nm:

$$S_A(\lambda) = 100 \left(\frac{\lambda_0}{\lambda}\right)^5 \frac{\exp\left(\frac{hc}{k\lambda_0 T_A}\right)}{\exp\left(\frac{hc}{k\lambda T_A}\right) - 1} \tag{27}$$

where $c \simeq 2.998 \times 10^8$ m.s^{-1} is the speed of light in vacuum, $h \simeq 6.626 \times 10^{-34}$ J.s is the Planck constant and $k \simeq 1.380 \times 10^{-23}$ J.K^{-1} is the Boltzmann constant.

The D series of illuminants were constructed by Judd, MacAdam, and Wyszecki to represent natural daylight [15]. The D50 and D65 illuminants are especially used in graphical industry and paper industry. Their spectra, plotted in Figure 7, are known to correspond to horizon daylight and

noon daylight spectra. They are easy to characterize mathematically since they may be derived from the linear combination of three spectra. However, they are difficult to produce artificially. Figure 8 shows two examples of light sources considered as D65 illuminants with noticeably different spectra: the light source in the SpectroEye spectrophotometer from X-rite and the 'Color Control Classic Line' light table from Just Normlicht. The F series of illuminants represent various types of fluorescent lighting. The ability of real light sources to reproduce the D65 illuminant can be assessed with the CIE metamerism index [16]. The F11 illuminant, plotted in Figure 7, is a narrow triband illuminant consisting of three narrowband emissions in the red, green and blue regions of the visible spectrum, obtained by a composition of rare-earth phosphors.
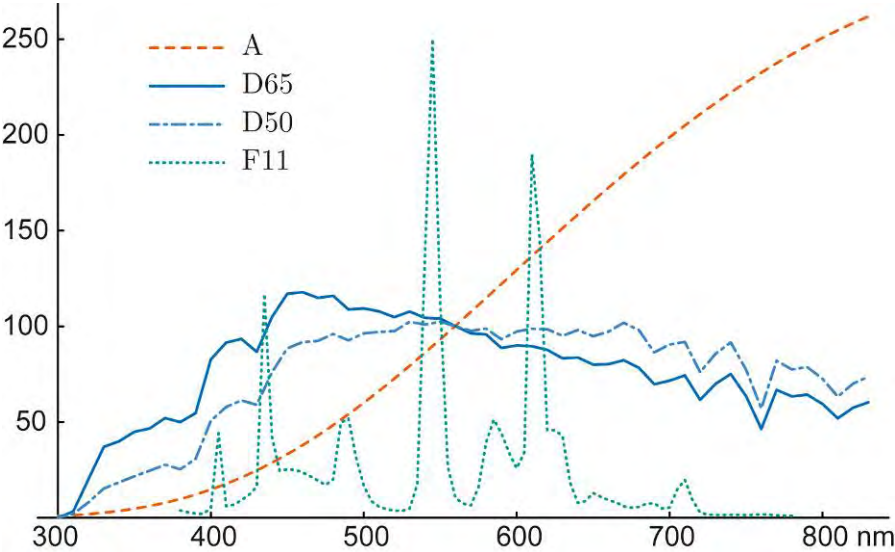

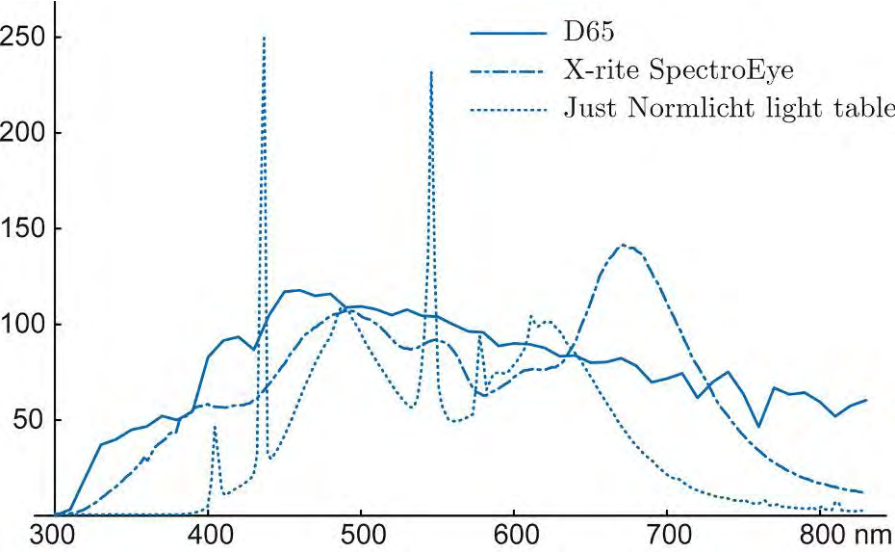Figure 7. Spectral distribution power of CIE standard illuminants A, D65, D50 and F11.

Figure 8. Spectrum of various light sources reproducing the D65 illuminant.

3.11. Measurement geometries

The reflectance measurement devices designed for color reproduction applications contain either directional or Lambertian white light source and capture the reflected light either in one direction (radiance measurement) or over the hemisphere thanks to an integrating sphere (irradiance measurement). The spectrum of the source generally tends to reproduce the color of a standard illuminant [29], typically the D65 illuminant, despite the difficulty to reproduce reliably the illuminant spectra defined by the CIE with artificial lightings (see Figure 8). Once captured, light is transferred to a spectrophotometer which measures the flux in the different wavelength bands 1, 5 or 10 nm wide. Table 1 presents some geometries recommended by the CIE for reflectance measurement [14].

Table 1. Some of the geometries recommended by the CIE for reflectance measurements

Appellation	Illumination	Capture
Diffuse / 8° geometry, specular component included (di:8°)	Diffuse	Radiance detector (8°)
Diffuse / 8° geometry, specular component excluded (de:8°)	Diffuse	Radiance detector (8°)
Diffuse / diffuse geometry (d:d)	Diffuse	Integrating sphere
Alternative diffuse geometry (d:0°)	Diffuse	Radiance detector (0°)
45° annular / normal geometry (45°a:0°)	Directional	Radiance detector (0°)
45° directional / normal geometry (45°x:0°)	Directional	Radiance detector (0°)

Integrating spheres are spherical cavities internally coated with a powder of nonabsorbing material, e.g. barium sulfate ($BaSO_4$), behaving as a perfect diffuser [30, 31]. They can be used either to produce a Lambertian illumination or to collect reflected light over the hemisphere. Figure 9 illustrates these two possibilities.
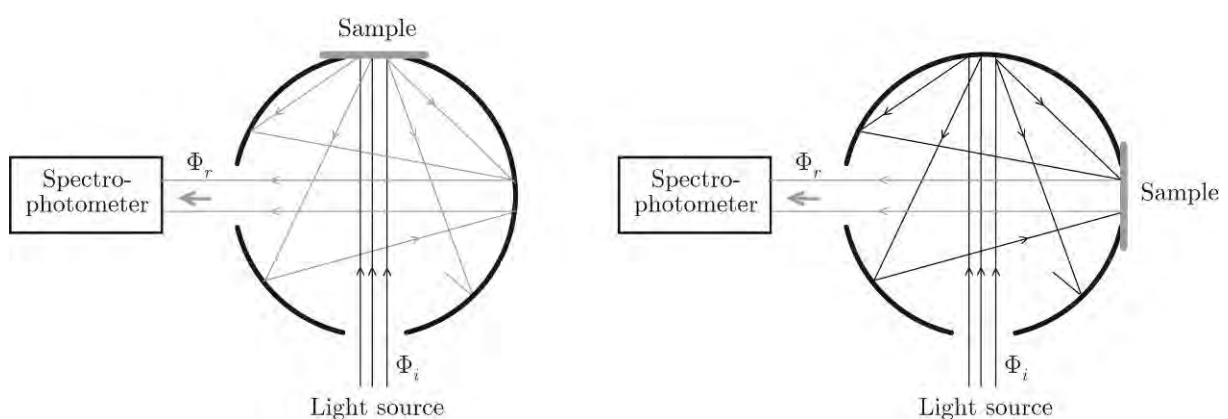

Figure 9. Integrating spheres used in a 0°:d geometry (left) and a d:0° geometry (right).

In the d:0°, the integrating sphere plays the role of diffuser for the illuminating flux. The reflected light is captured at 0° or 8° in respect to the normal of the sample. In the case of diffusing samples

having a flat surface, one may want to discard the specular reflection component from the measurement. A hole located in the regular direction in respect to the detector position ensures that the specular reflection component is not captured [18]. A hemispherical-directional reflectance is measured. In the 0°:d geometry, the integrating sphere collects the whole flux reflected by the sample, which is illuminated by a collimated beam. The corresponding reflectance is a "directional reflectance", given by equation (21).

In contrast with integrating spheres, radiance detectors capture only a fraction of the flux issued from the specimen. This fraction depends on both area and solid angle of the detector, which are generally unknown. The so-called 45°:0° geometry, widely used in the printing industry, is a bidirectional geometry where light is incident at 45° and a radiance detector captures light at 0° [31]. The sample is illuminated from one or all azimuth directions, yielding respectively the *directional* and *annular* variants of the 45°:0° geometry. The annular geometry, illustrated by Figure 10, minimizes texture and directionality whereas the directional geometry tends to enhance them.
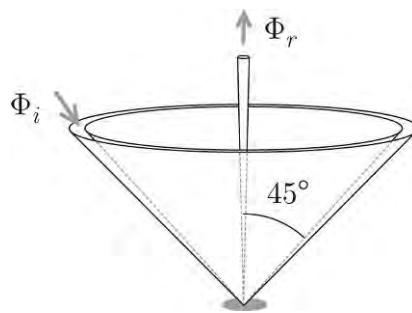

Figure 10. 45° annular / normal geometry (45°a:0°) for reflectance measurements.

Several companies such as X-rite, Datacolor and Konica Minolta have developed spectrophotometers able to measure both reflectance and transmittance. They are typically based on the di:8° and de:8° geometry in reflectance mode, and on the d°:0° geometry in transmittance mode. Note that all these measurement geometries make sense when the sample is diffusing. Using them with nonscattering sample, either in reflectance or transmittance mode, needs some precaution. For example, when measuring the transmittance of a nonscattering filter with a d:0 geometry, only the radiance normal to the sample is captured by the detector (Figure 11). The effective measurement geometry is therefore the 0:0 geometry. The incident radiance at 0° is obtained by measurement without the sample. Thus, ratio of measurements with the sample and without it provides the directional transmittance at 0°. We have similar configuration with a mirror using a d:8 geometry in reflectance mode, where the effective geometry is the 8:8 geometry. The incident radiance is obtained by performing a measurement on a reference mirror whose spectral reflectance is perfectly known. As an alternative, it can be obtained from a

measurement of a perfect non-absorbing diffuser: the radiance reflected at 8° coincides with the radiance incident at 8° on the mirror (E/π in both cases, where E is the total incident irradiance). In the case of weakly scattering samples, however, the amount of incident light being able to reach the detector cannot be certainly known since it depends on the scattering diagram of the medium. The reflectance and reflectance factor concepts have no pertinence any more. Only BRDF and BTDF measurement can provide reliable information on the reflecting and transmitting properties of the sample.
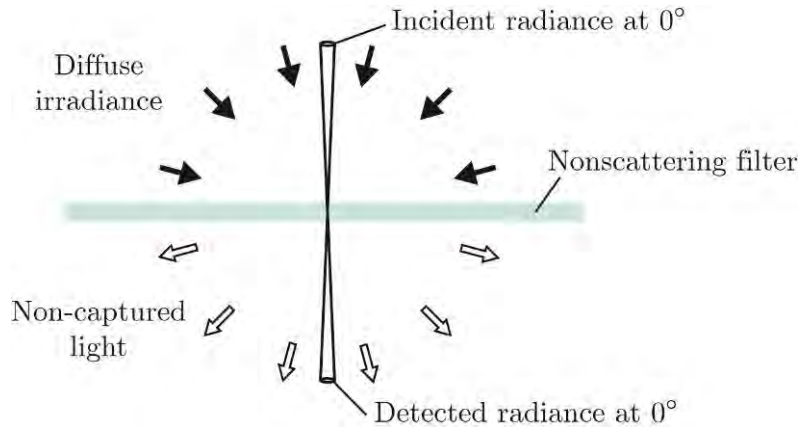

Figure 11. Transmittance measurement of a nonscattering filter with a d:0 geometry. Only the radiance incident at 0° is captured and the light coming from other directions is ignored by the detector. The effective measurement geometry is the 0:0 geometry.

4. REFLECTION AND REFRACTION

Two media of different refractive indices have in common a planar boundary called *interface*. The optical properties of the interface depend on its *relative refractive index*, i.e. the ratio of the refractive indices of the two media. When the interface is flat, each of its faces reflects and transmits unidirectional light into one couple of directions, called *regular* or *specular directions*, attached to the reflected and refracted components. Reflection and refraction play an important role in the interaction of light with printed supports. Everyone has observed the reflection of light by the surface of a glossy photograph. At the other side of the surface, the diffuse light coming from the paper and the inks is also reflected. Thus, light travels several times in average between the paper substrate and the inks before exiting the print definitively.

4.1. Refractive index

The refractive index of a medium is a measure of the propagation properties of light in that medium. It is generally a complex number depending on wavelength:

$$\hat{n}(\lambda) = n(\lambda) + i\kappa(\lambda) \tag{28}$$

The real part $n(\lambda)$, called *real refractive index*, is related with the light propagation speed. The imaginary part $\kappa(\lambda)$, called *extinction index*, characterizes absorption by the medium. Table 2 gives the refractive indices of a few common materials.

Table 2. Refractive indices of materials measured at $\lambda = 589$ nm (Sodium D line)

Air [a]	1.0003
Water (at 20°C) [a]	1.333
Ethanol [a]	1.36
Fused quartz SiO_2	1.45
Cellulose	1.47
Polypropylene	1.49
Acrylic [b]	1.49
Polyvinyl alcohol	1.50
Plexiglass	1.51
Crown glass [a]	1.52
Sodium Chloride (NaCl) [a]	1.544
Amber [a]	1.55
Polycarbonate [b]	1.58
Polystyrene [a]	1.59
Zircon ($ZrO_2 \cdot SiO_2$) [a]	1.923
Diamond [a]	2.417
Rutile (TiO_2) [a]	2.907
Gold	$0.27 + 2.95\,i$
Silver [c]	$0.20 + 3.44\,i$
Copper [c]	$0.62 + 2.57\,i$
Platinum [c]	$2.63 + 3.54\,i$
Aluminium [c]	$1.44 + 5.23\,i$

[a] Reference [37], p. 95. [b] Reference [35], p. 828. [c] Reference [2], p. 747.

Ellipsometry is the favourite technique for refractive index measurements. It is based on polarization analysis. The constraint is that the sample must be homogenous, nonscattering and very flat, which makes this technique almost impossible to use with printing materials such as inks and paper. Note that the real and imaginary functions of wavelength are related to each other by the Kramers-Kronig relations [32, 33, 34]. Thus, knowing either the real index or the extinction index over the whole spectrum enables obtaining the other one for any wavelength.

For dielectric materials such as glass, plastic or paper fibres, the attenuation index is low compared to the real index. The refractive index may be considered as being real and absorption is modelled independently by an attenuation factor applied to the ray (*see* the section on Beer's law). The dependence of the real index on wavelength, being at the origin of the *dispersion* phenomenon [33] as well as the chromatic aberrations in optical systems [35], is empirically modelled in the visible wavelength domain by Cauchy's law [2, 36]:

$$n(\lambda) = a_1 + \frac{a_2}{\lambda^2} \tag{29}$$

where the dimensionless factor a_1 and the coefficient a_2 (in m^{-2}) are to be determined for each medium. As the real index varies with respect to wavelength, rays are refracted at different angles and split white light pencils into diverging pencils, commonly called *rainbows* in the case of rain drops. However, dispersion has no significant effect when the incident light is diffuse or when the medium is diffusing, because the different spectral components superpose to each other and yield again white light in all directions. This is the reason why dispersion is ignored in the case of papers or white paints and a constant real refractive index is attached to them.

4.2. Snell's laws

When a light ray propagating into a given medium 1 encounters a medium 2 with different refractive index, its orientation is modified: a component is reflected back into medium 1, and a second component is refracted into medium 2. The directions of reflection and refraction satisfy *Snell's laws*: 1) the incident, reflected and refracted light rays belong to a same plane, called the *incidence plane*, which also contains the normal of the interface; 2) the angles formed by the incident ray and the reflected ray with respect to the normal of the interface are equal; 3) the angle of refraction is related to the angle of incidence according to the "sine law"

$$n_1 \sin \theta_1 = n_2 \sin \theta_2 \tag{30}$$

where n_1 and n_2 denote the refractive indices of the two media and θ_1 and θ_2 the respective orientations of light in them (Figure 12).
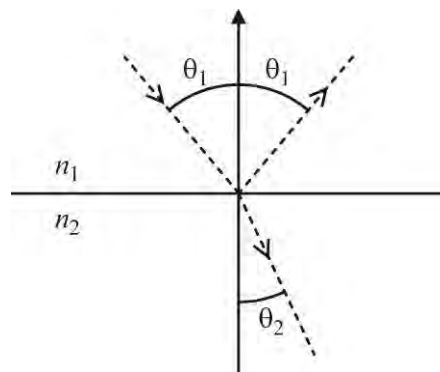

Figure 12. Reflection and refraction in the incidence plane, when $n_1 < n_2$.

Note that the wavelength of light is modified when entering the second medium. The wavelength concept is therefore dependent upon the propagation medium, being shorter in the medium with higher index. However, as light sources and detectors are generally in air, all detected rays have

their original wavelength even after having traversed different media. Wavelength variation in matter is therefore ignored and only the wavelength in air is considered.

4.3. Total reflection

Let us assume $n_1 < n_2$. When light comes from medium 1, the refraction angle is always smaller than the incidence angle. At grazing incidence, i.e. $\theta_1 = \pi/2$, the refraction angle reaches a limit value $\theta_c = \arcsin(n_1/n_2)$, called the *critical angle*. No light can be refracted into medium 2 with higher angle. When light comes from medium 2, it is refracted into medium 1 provided the incident angle θ_2 is lower than the critical angle θ_c. Otherwise, Snell's sine law (30) provides no real solution for angle θ_1, refraction does not occur and the ray is totally reflected.

4.4. Fresnel's formulae

The fraction of light that is reflected by the interface between media 1 and 2 is called *angular reflectance*. It is given by Fresnel's formulae, established by writing the transition equation of electromagnetic waves at the interface. It depends on the incident angle θ_1, on the relative refractive index of the interface $n = n_2/n_1$ and on the polarization of the incident light. Most of the time, we consider unpolarized incident light which is modelled as the sum of two linearly polarized lights (see Section 1.2). Since the angular reflectance depends on the orientation of the electric field in respect to the incidence plane, we consider the cases where the electric field oscillates parallely and perpendicularly to the incidence plane. These two polarizations are respectively called "parallel" and "perpendicular" polarizations and denoted by symbols *p* and *s*.

Let us consider a light pencil coming from medium 1 with incident angle θ_1. For *p*-polarized light, the angular reflectance is

$$R_{p12}(\theta_1) = \left(\frac{\tan(\theta_1 - \theta_2)}{\tan(\theta_1 + \theta_2)}\right)^2 = \left(\frac{n\cos\theta_1 - \cos\theta_2}{n\cos\theta_1 + \cos\theta_2}\right)^2 \tag{31}$$

where $\theta_2 = \arcsin(n_1 \sin\theta_1/n_2)$ is the angle of refraction into medium 2 defined by Snell's law. For *s*-polarized light, the angular reflectance is

$$R_{s12}(\theta_1) = \left(\frac{\sin(\theta_1 - \theta_2)}{\sin(\theta_1 + \theta_2)}\right)^2 = \left(\frac{\cos\theta_1 - n\cos\theta_2}{\cos\theta_1 + n\cos\theta_2}\right)^2 \tag{32}$$

The variation of angular reflectance for the *p*- and *s*-polarized components are plotted in Figure 13 as a function of the incident angle θ_1 for an interface with relative refractive index $n = 1.5$.

At normal incidence, *p*-polarized, *s*-polarized and unpolarized lights have the same angular reflectance:

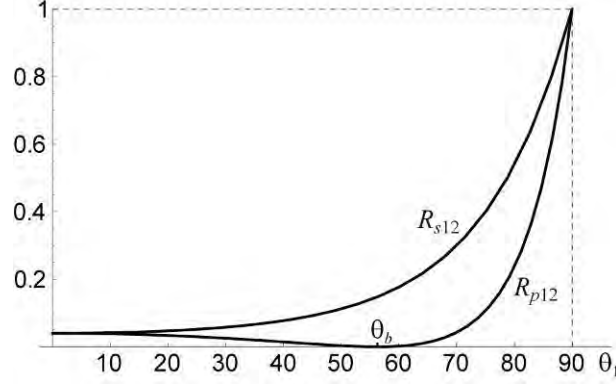$$R_{p12}(0) = R_{s12}(0) = R_{12}(0) = \left(\frac{n-1}{n+1}\right)^2 \tag{33}$$

Figure 13. Angular reflectance for *p*- and *s*-polarized lights when $n = n_2 / n_1 = 1.5$. The Brewster angle is $\theta_b = \arctan(1.5) \approx 56.3°$.

For oblique incidence, angular reflectances may expressed as functions of angle θ_1 only, by inserting $\theta_2 = \arcsin(\sin \theta_1 / n)$ into equations (31) and (32):

$$R_{p12}(\theta_1) = \left(\frac{n^2 \cos \theta_1 - \sqrt{n^2 - \sin^2 \theta_1}}{n^2 \cos \theta_1 + \sqrt{n^2 - \sin^2 \theta_1}} \right)^2 \tag{34}$$

$$R_{s12}(\theta_1) = \left(\frac{\cos \theta_1 - \sqrt{n^2 - \sin^2 \theta_1}}{\cos \theta_1 + \sqrt{n^2 - \sin^2 \theta_1}} \right)^2 \tag{35}$$

Unpolarized light contains same quantity of *p*- and *s*-polarizations. Therefore, the angular reflectance for unpolarized light is the average of the two angular reflectances:

$$R_{12}(\theta_1) = \frac{1}{2} \left[R_{p12}(\theta_1) + R_{s12}(\theta_1) \right] \tag{36}$$

Except at normal incidence, the *p*- and *s*-polarized lights are reflected in different proportions. The reflected and transmitted lights are therefore partially polarized. At the angle $\theta_b = \arctan(n_{12})$, called the *Brewster angle*, *p*-polarized light is not reflected at all. The corresponding angular reflectance is zero. The reflected light is therefore totally polarized (s-polarization). Reflection at the Brewster angle is one possible method to produce linearly polarized light.

Independently of polarization, the angular reflectance is the same if light comes from medium 1 at the angle θ_1 or comes from medium 2 at the corresponding regular angle $\theta_2 = \arcsin(n_1 \sin \theta_1 / n_2)$:

$$R_{*12}(\theta_1) = R_{*21}(\theta_2) \tag{37}$$

where symbol $*$ means either *s*-polarized, *p*-polarized or unpolarized light. Figure 14 shows the variation of angular reflectances and transmittances from normal to grazing incidence in both medium 1 and 2 for an interface with relative index $n = 1.5$.
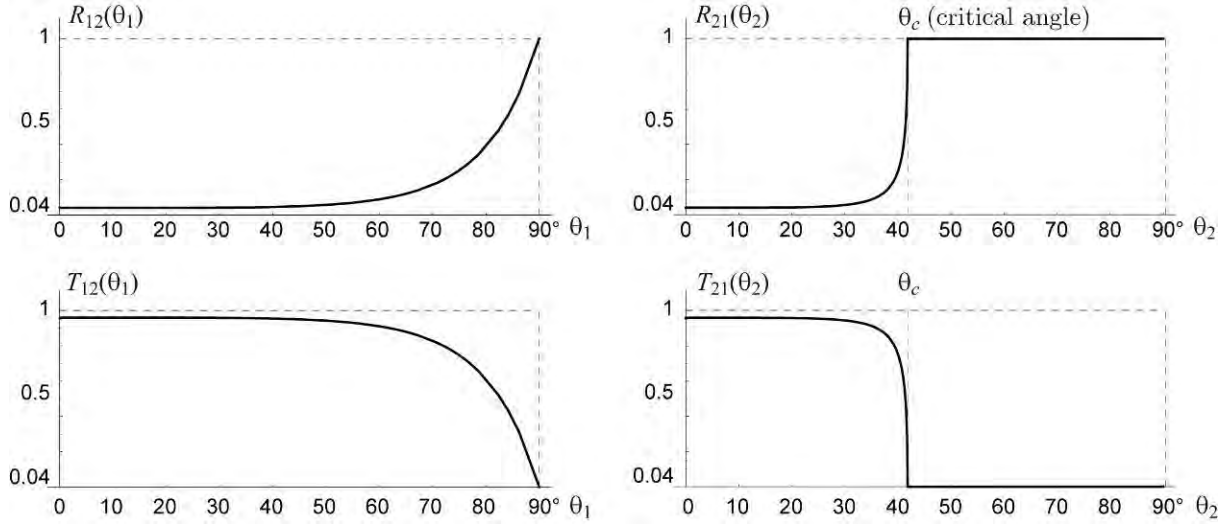
Figure 14. Angular reflectance and transmittance of an interface with relative index $n = n_2 / n_1 = 1.5$ as a function of the incident angle for natural light from medium 1 (*left*) or medium 2 (*right*).

Regarding the refracted component, since no light is absorbed at the interface, the *angular transmittance* is

$$T_{*12}(\theta_1) = 1 - R_{*12}(\theta_1)$$ (38)

and, as a consequence of (37), one has

$$T_{*12}(\theta_1) = T_{*21}(\theta_2)$$ (39)

This equality means that for a given path of light, the angular transmittance does not depend whether light transits from medium 1 to medium 2 or from medium 2 to medium 1. In case of total reflection, the angular transmittance is zero.

4.5. Radiance reflection and refraction

In radiometry, light pencils are described by the radiance concept. When a pencil enters a medium with different index, refraction modifies the ray's geometrical extent (Figure 15). Radiance is thus modified. The relationship between incident, reflected and refracted radiances is derived from geometrical arguments issued from Snell's laws.

The incident radiance L_1 is defined as the flux element $d^2\Phi_1(\theta_1, \varphi_1)$ coming from direction (θ_1, φ_1) through the infinitesimal solid angle $d\omega_1 = \sin\theta_1 d\theta_1 d\varphi_1$, and illuminating a an elemental area ds

$$L_1 = \frac{d^2\Phi_1(\theta_1, \varphi_1)}{ds\cos\theta_1 \sin\theta_1 d\theta_1 d\varphi_1}$$ (40)
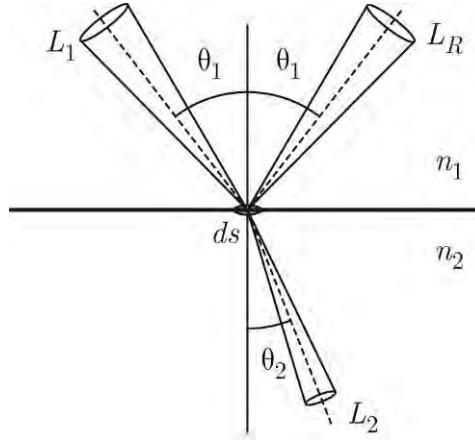
Figure 15. Incident, reflected and refracted radiances at the interface between two media of indices n_1 and $n_2 > n_1$.

The denominator in equation (40) denotes the geometrical extent of the incident pencil. Since the reflected and incident pencils form the same angle with the normal, they have the same geometrical extent. The reflected radiance L_R is therefore the incident radiance L_1 attenuated by the angular reflectance $R_{12}(\theta_1)$ of the interface

$$L_R = R_{12}(\theta_1)L_1 \tag{41}$$

Regarding the refracted pencil, the refraction and incidence angles satisfy Snell's sine law (30). By differentiating equation (30), one obtains

$$n_1 \cos\theta_1 d\theta_1 = n_2 \cos\theta_2 d\theta_2 \tag{42}$$

The incident and refracted azimuthal angles form a fixed angle π, a small variation of the one implies the same variation of the other one, i.e. $d\varphi_1 = d\varphi_2$. Hence, one has

$$n_1^2 ds \cos\theta_1 \sin\theta_1 d\theta_1 d\varphi_1 = n_2^2 ds \cos\theta_2 \sin\theta_2 d\theta_2 d\varphi_2 \tag{43}$$

i.e.

$$n_1^2 dG_1 = n_2^2 dG_2 \tag{44}$$

where dG_1 and dG_2 denote the geometrical extent of the pencil in media 1 and 2 respectively. Equation (44) shows that the geometrical extent is multiplied by a factor $(n_j/n_i)^2$ each time it goes from a medium i to a medium j, but the quantity $n_i^2 dG_i$ remains invariant. This invariance generalizes the invariance of geometrical extent stated in the previous section in the special case where the extremities of the pencil where both located in air. Finally, accounting for the changing of geometrical extent due to the refraction, the refracted radiance is

$$L_2 = (n_2/n_1)^2 T_{12}(\theta_1)L_1 \tag{45}$$

4.6. Lambertian reflectance of an interface

Let us now consider that the interface is illuminated by Lambertian light. We denote as $n = n_2 / n_1$ the relative index of the interface and assume that $n > 1$. When the light comes from medium 1, the "Lambertian reflectance", denoted as r_{12}, is given by equation (22)

$$r_{12} = \int_{\theta_1=0}^{\pi/2} R_{12}(\theta_1) \sin 2\theta_1 d\theta_1 \tag{46}$$

r_{12} depends only on the relative index n. It may be computed by discrete summation with a small sampling step, e.g. $\Delta\theta_1 = 0.001$ rad. Alternatively, it is given by the following analytical formula [38]

$$r_{12} = \frac{1}{2} + \frac{(n-1)(3n+1)}{6(n+1)^2} - \frac{2n^3(n^2+2n-1)}{(n^4-1)(n^2+1)} + \frac{8n^4(n^4+1)\ln(n)}{(n^4-1)^2(n^2+1)} + \frac{n^2(n^2-1)^2}{(n^2+1)^3} \cdot \ln\left(\frac{n-1}{n+1}\right) \tag{47}$$

The reflected flux fulfills the whole hemisphere but is not Lambertian anymore as the reflected radiance varies with angle. The transmitted flux is concentrated into the cone delimited by the critical angle $\theta_c = \arcsin(1/n)$. The conservation of the energy at the interface implies that the transmittance is

$$t_{12} = 1 - r_{12} \tag{48}$$

When the Lambertian light comes from medium 2, the reflectance r_{21} is similarly expressed as r_{12} with $R_{12}(\theta_1)$ replaced by $R_{21}(\theta_2)$

$$r_{21} = \int_{\theta_2=0}^{\pi/2} R_{21}(\theta_2) \sin 2\theta_2 d\theta_2 \tag{49}$$

Even though $R_{12}(\theta_1)$ and $R_{21}(\theta_2)$ are equal [*see* equation (37)], reflectances r_{12} and r_{21} are different due to total reflection which takes place in medium 2 but not in medium 1. They are related by the following formula established in Appendix A.1:

$$1 - r_{21} = \frac{1}{n^2}(1 - r_{12}) \tag{50}$$

One deduces from it the relationship of transmittances:

$$t_{21} = \frac{1}{n^2} t_{12} \tag{51}$$

For an air-glass interface of typical relative index $n = 1.5$, one has $r_{12} \simeq 0.1$, $t_{12} \simeq 0.9$, $r_{21} \simeq 0.6$ and $t_{21} \simeq 0.4$. Their values for other indices are listed in [39] and in Appendix B.3.

4.7. Absorbing media and metals

The color of a homogenous medium comes from its capacity to absorb radiations of specific wavelengths in the visible domain, which corresponds to a nonzero extinction index $\kappa(\lambda)$. The absorption coefficient α is related to the extinction index by the formula [2]

$$\alpha(\lambda) = \frac{4\pi}{\lambda}\kappa(\lambda) \tag{52}$$

This relation is valid for any absorbing medium, e.g. colored glass or metal. The particularity of metals is their high extinction index, which makes them very opaque and reflecting. The angular reflectance of air-metal interfaces is given by the same Fresnel formulas (31) and (32) as for air-dielectric interfaces, but the refractive index is a complex number $\hat{n} = n + i\kappa$ including the extinction coefficient [2]. The refraction angle θ_2 is also a complex number. Nevertheless, the angular reflectance is real and may be expanded as follows:

$$R_{s12}(\theta_1) = \frac{\left(\sqrt{a+z} - \sqrt{2}\cos\theta_1\right)^2 + a - z}{\left(\sqrt{a+z} + \sqrt{2}\cos\theta_1\right)^2 + a - z} \tag{53}$$

$$R_{p12}(\theta_1) = R_{s12}(\theta_1) \cdot \frac{\left(\sqrt{a+z} - \sqrt{2}\sin\theta_1\tan\theta_1\right)^2 + a - z}{\left(\sqrt{a+z} + \sqrt{2}\sin\theta_1\tan\theta_1\right)^2 + a - z} \tag{54}$$

with $z = n^2 - \kappa^2 - \sin^2\theta_1$ and $a = \sqrt{z^2 + 4\kappa^2{}^2}$. For unpolarized incident light, the angular reflectance is the average of formulas (53) and (54).
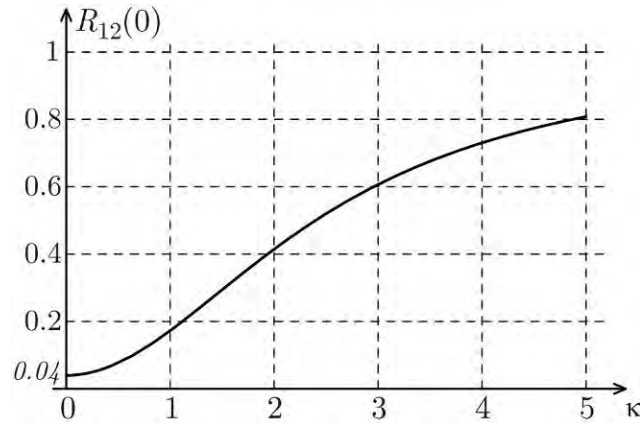
Figure 16. Variation of the angular reflectance at normal incidence of an interface with relative refractive index $\hat{n} = 1.5 + i\kappa$ as a function of κ.

Figure 16 illustrates how the angular reflectance increases as the extinction coefficient increases. From $\kappa = 0$ to 0.2, the angular reflectance remains close to 0.04, i.e. the value corresponding to a real index of 1.5. This justifies that for weakly absorbing dielectrics the extinction index is not

taken into account in the Fresnel formulas. Beyond 0.2, the angular reflectance increases rapidly. On a spectral point of view, the angular reflectance a surface is higher at the wavelengths where the medium is the more absorbing (higher absorption coefficient). Reflected and transmitted lights therefore get complementary colors.
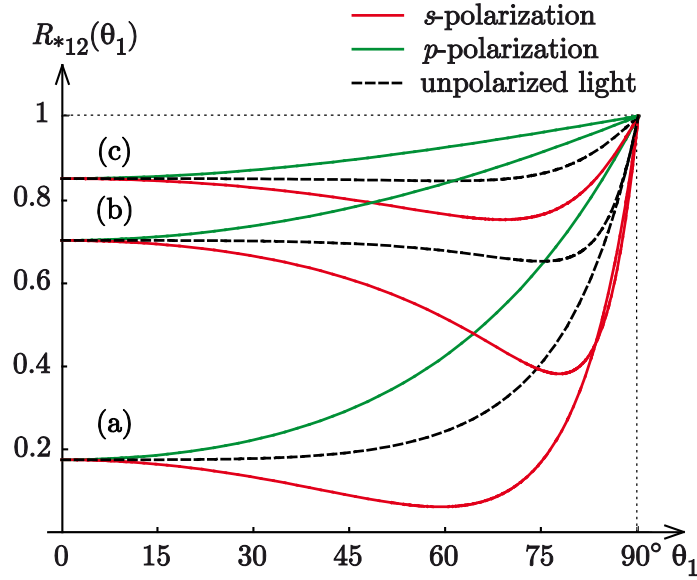

Figure 17. Angular reflectance as a function of the incident angle, for *p*-polarized, *s*-polarized and unpolarized lights, of (a) strongly absorbing glass ($\hat{n} = 1.5 + i$), (b) platinum at 589 nm ($\hat{n} = 2.06 + 4.26i$) and (c) gold at 600 nm ($\hat{n} = 0.37 + 2.82i$).

The variation of the angular reflectance as a function of the incident angle is noticeably different between absorbing media and nonabsorbing media. Figure 17 shows three examples based on the refractive indices of a strongly absorbing glass ($\hat{n} = 1.5 + i$), gold at 600 nm ($\hat{n} = 0.37 + 2.82i$) and platinum at 589 nm ($\hat{n} = 2.06 + 4.26i$). In the three cases, the angular reflectance for *s*-polarized light is a strictly increasing function of the incident angle, while the one for *p*-polarized light decreases to a minimum without reaching zero. The reflected light is therefore partially polarized but there is no angle at which its polarization is total. In the case of gold and platinum, the angular reflectance for unpolarized light reaches a minimum, whereas the minimum is at normal incidence for dielectrics.

5. ABSORPTION

Absorption denotes the attenuation of light due to the conversion of the electromagnetic energy into another form of energy, typically because its frequencies are resonant with transition frequencies of the atoms in the medium [36]. The attenuation factor depends on the optical length traveled in the medium. It is given by the Beer-Lambert law. Absorption may be strongly

dependent upon wavelength. It is responsible for the colored aspect of most objects, such as stained glasses, dyes, pigments, and inks.

5.1. Transmittance of an absorbing layer

The absorbing power of a medium is assessed by its absorption coefficient $\alpha(\lambda)$, in m^{-1}, which depends upon wavelength and is related to the extinction coefficient of the medium according to relation (52). According to Beer's law, light is exponentially attenuated in this medium as a function of the path length. When a light beam crosses a layer of this medium with thickness h, the attenuation, called *normal transmittance*, is given by

$$t = e^{-\alpha h}$$

If the beam crosses the layer at an angle θ to the normal, the travelled distance in the layer becomes $h/\cos\theta$ (see Figure 18) and the attenuation $T(\theta)$ becomes:

$$T(\theta) = e^{-\alpha h/\cos\theta} = t^{1/\cos\theta} \tag{55}$$

$T(\theta)$ is the "directional transmittance" of the layer, following the definition of "directional reflectance" given in Section 3.7. The "Lambertian transmittance" is expressed by an similar integral as in equation (22)

$$T = \int_{\theta=0}^{\pi/2} T(\theta)\sin 2\theta d\theta = \int_{\theta=0}^{\pi/2} t^{1/\cos\theta} \sin 2\theta d\theta \tag{56}$$
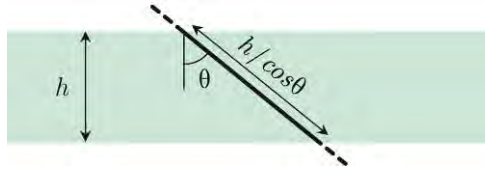

Figure 18. Path travelled through a layer with thickness h by directional light oriented by an angle θ from the normal.

When different transparent layers with identical refractive indices are superposed, they form again an absorbing, nonscattering layer whose normal transmittance is the product of their individual normal transmittances. The oblique transmittance of the layer is also the product of the individual oblique transmittances considered at the same angle. Regarding the multilayer's Lambertian transmittance, it is expressed by the same integral as in equation (56) where $T(\theta)$, in this case, represent the directional transmittance of the multilayer at angle θ. It can be expressed in terms of the normal transmittances t_1, t_2, t_3,... of the different layers:

$$T = \int_{\theta=0}^{\pi/2} (t_1 t_2 t_3 ...)^{1/\cos\theta} \sin 2\theta d\theta \tag{57}$$

but not in terms of the Lambertian transmittances of the individual layers:

$$T \neq \int t_1^{1/\cos\theta} \sin 2\theta d\theta \int t_2^{1/\cos\theta} \sin 2\theta d\theta \dots$$

5.2. Reflectance and transmittance of an absorbing film

Color filters and stained glasses are examples of absorbing layers in which light is exponentially attenuated according to Beer's law. However, since the layer is surrounded by air, its surfaces refract and reflect light and a multiple reflection process takes place within them. Consequently, some light is reflected by the film and the global absorption is increased. We want to determine the film's reflectance and the transmittance for natural incident light being at first collimated, then Lambertian.

Let us denote as t the normal transmittance of a film considered without interfaces, and n_2 its refractive index. The interfaces with air ($n_1 = 1$) are assumed to be flat and parallel. The film's thickness is significantly larger than the *coherence length* of the incident white light, which is ordinarily a few micrometers [36]. Interferences can therefore be ignored. In the opposite case, the film would be considered as a *thin film* and its interaction with light should be described by wave optics [40].
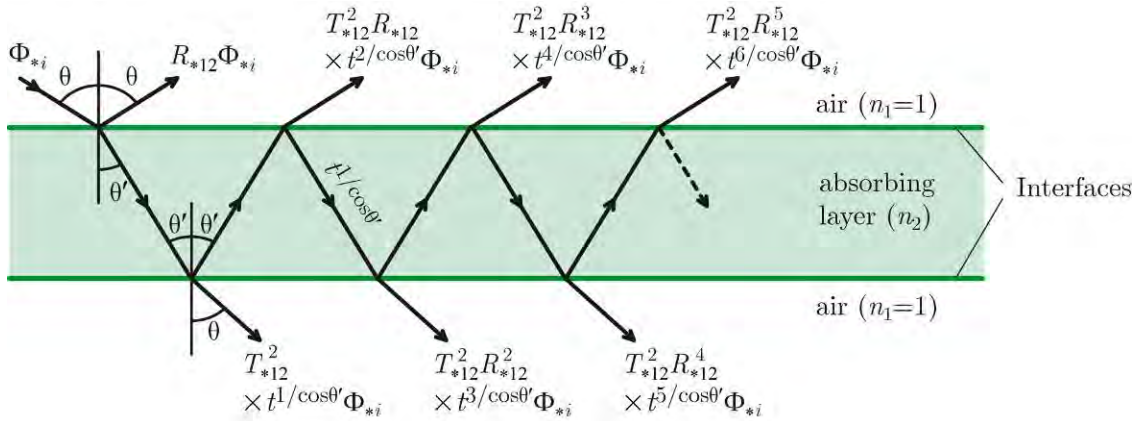
Figure 19: Multiple reflections of light in an absorbing plate.

When the incoming pencil strikes the front surface, it splits into reflected and refracted pencils. The refracted pencil reaches the back surface where it splits again into reflected and refracted components. The reflected component again splits at the front surface into reflected and transmitted components and so on. We have a multiple reflection process as described by Figure 19. The two polarized components follow the same trajectories in the layer, which all belong to the incidence plane and form with the normal an angle θ in air and an angle θ' in the layer. The two angles are related by Snell's sine law

$$\sin\theta = n \sin\theta' \qquad (58)$$

with $n = n_2/n_1 \simeq n_2$. According to the Fresnel formulas, the surfaces' angular reflectance and transmittance are different for the p and s-polarized lights. Let us denote as $R_{*12}(\theta)$ the angular reflectance corresponding to reflection at angle θ in air, where the symbol "$*$" means "either p or s". Recall from equation (37) that the rays coming from the layer at the angle θ' have the same angular reflectance. The corresponding angular transmittance is $T_{*12}(\theta) = 1 - R_{*12}(\theta)$.

Being given the incident angle θ of the p- or s-polarized flux Φ_{*i}, we want to determine the fluxes Φ_{*r} and Φ_{*t} exiting respectively at the front side and the back side. At the front surface, Φ_{*i} splits into a reflected flux $R_{*12}(\theta)\Phi_{*i}$ and a transmitted flux $T_{*12}(\theta)\Phi_{*i}$. The transmitted flux travels a distance $h/\cos\theta'$ in the layer and is attenuated by a factor $t^{1/\cos\theta'}$ [see equation (55)], then splits at the back surface into a reflected flux $T_{*12}(\theta)R_{*12}(\theta)t^{1/\cos\theta'}\Phi_{*i}$ and a transmitted flux $T_{*12}^2(\theta)t^{1/\cos\theta'}\Phi_{*i}$ which exits definitely the plate at the back side. The reflected flux is again attenuated by a factor $t^{1/\cos\theta'}$ while crossing the layer, then reaches the upper surface where it splits into a reflected component $T_{*12}(\theta)R_{*12}^2(\theta)t^{2/\cos\theta'}\Phi_{*i}$ and a transmitted component $T_{*12}^2(\theta)R_{*12}(\theta)t^{2/\cos\theta'}\Phi_{*i}$ which exits the plate at the front side. By pursuing the description of the multiple reflection process, we obtain the different fluxes exiting the plate at the upper and lower sides, the first ones being given in Figure 19. The total reflected and transmitted fluxes are expressed by the following infinite sums

$$\Phi_{*t} = T_{*12}^2(\theta)t^{1/\cos\theta'}\sum_{k=0}^{\infty}\left[R_{*12}^2(\theta)t^{2/\cos\theta'}\right]^k\Phi_{*i},$$

$$\Phi_{*r} = R_{*12}(\theta)\Phi_{*i} + T_{*12}^2(\theta)R_{*12}(\theta)t^{2/\cos\theta'}\sum_{k=0}^{\infty}\left[R_{*12}^2(\theta)t^{2/\cos\theta'}\right]^k\Phi_{*i} \qquad (59)$$

which are geometrical series. The exponents $1/\cos\theta'$ can be expressed as function of angle θ using the following relation issued from Snell's law:

$$\cos\theta' = \sqrt{1 - (\sin\theta/n)^2} \qquad (60)$$

Finally, the ratio of reflected (respectively transmitted) flux to incident flux gives the reflectance (respectively the transmittance) of the plate for the considered polarization:

$$R_*(\theta) = R_{*12}(\theta) + \frac{T_{*12}^2(\theta)R_{*12}(\theta)t^{2/\sqrt{1-(\sin\theta/n)^2}}}{1 - R_{*12}^2(\theta)t^{2/\sqrt{1-(\sin\theta/n)^2}}} \qquad (61)$$

and

$$T_*(\theta) = \frac{T_{*12}^2(\theta)t^{1/\sqrt{1-(\sin\theta/n)^2}}}{1 - R_{*12}^2(\theta)t^{2/\sqrt{1-(\sin\theta/n)^2}}} \qquad (62)$$

For natural light, the total reflectance and transmittance of the plate at angle θ are the average of the reflectances, respectively transmittances attached to the two polarizations, i.e.

$$R(\theta) = \frac{1}{2}\left[R_p(\theta) + R_s(\theta)\right] \quad \text{and} \quad T(\theta) = \frac{1}{2}\left[T_p(\theta) + T_s(\theta)\right] \tag{63}$$

At normal incidence, with the angular reflectance $R_{*12}(\theta)$ given by equation (33), the reflectance and transmittance of the plate become

$$R(0) = \frac{8n(1-n)^2 t^2}{(1+n)^4 - (1-n)^4 t^2} \tag{64}$$

and

$$T(0) = \frac{16n^2 t}{(1+n)^4 - (1-n)^4 t^2} \tag{65}$$

where $n = n_2 / n_1$. The transmittance formula is especially used to assess spectral transmission by colored filters (*see* Reference [18], p. 30). By inverting it, we can obtain the normal transmittance t from the transmittance measured at normal incidence:

$$t = \frac{\sqrt{64n^4 + (1-n^2)^4 T^2(0)} - 8n^2}{(1-n)^4 T(0)} \tag{66}$$

As the incident light moves away from the normal, the *s*-polarized light is more reflected than the *p*-polarized light (see Figure 20). Consequently, if the incident light is unpolarized, the reflected and transmitted lights become partially polarized. According to the formula (1), the degree of polarization of the reflected light is

$$DOP = \left| \frac{R_s(\theta) - R_p(\theta)}{R_s(\theta) + R_p(\theta)} \right| \tag{67}$$

The variation of the DOP as a function of the incident angle is plotted in Figure 17. It is 0 at normal incidence, grows to 1 at the Brewster angle then returns to 0 at grazing incidence. This means that the reflected light remains unpolarized at normal and grazing incidences and is totally s-polarized at the Brewster angle.

In color reproduction, polarization is often ignored, which comes to consider that light is unpolarized at each reflection and refraction (see for example [41]). This yields similar reflectance and transmittance expressions as in equations (61) and (62), except that $R_{*12}(\theta)$ represents in this case the surfaces' angular reflectance for natural light:

$$R_u(\theta) = \frac{2T_{12}^2(\theta)R_{12}(\theta)t^{2/\sqrt{1-(\sin\theta/n)^2}}}{1 - R_{12}^2(\theta)t^{2/\sqrt{1-(\sin\theta/n)^2}}} \quad \text{and} \quad T_u(\theta) = \frac{T_{12}^2(\theta)t^{1/\sqrt{1-(\sin\theta/n)^2}}}{1 - R_{12}^2(\theta)t^{2/\sqrt{1-(\sin\theta/n)^2}}} \tag{68}$$

The variation of this reflectance $R_u(\theta)$ for a nonabsorbing plate of refractive index 1.5 is plotted in Figure 20. We see that it deviates noticeably from the reflectance of an ideal plate given by equation (63) and is not valid for glass plates. However, it may happen with some kinds of

plastics that DOP is strongly decreased by loss of light's coherence during the multiple reflection process [3], generally due to heterogeneities in the medium or the surfaces.
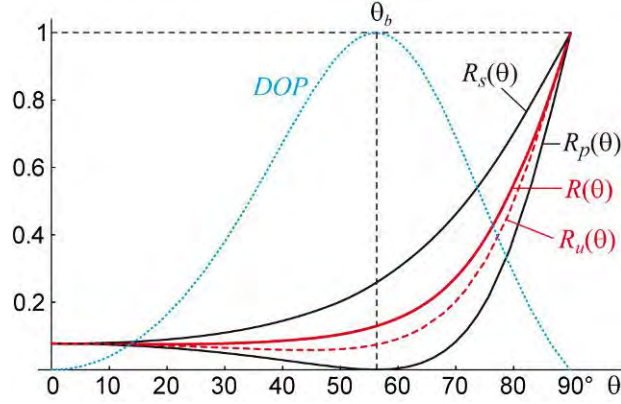

Figure 20. Directional reflectance of a nonabsorbing plate of refractive index 1.5 for the parallely polarized light, perpendicularly polarized light and natural light according to the model accounting for polarization, and directional reflectance ignoring polarization. The Brewster angle is $\theta_b = \arctan(n_2 / n_1) \simeq 56.3°$.

When the incident irradiance is Lambertian, the plate's reflectance and transmittance are given by similar formulas as for a single interface [*see* equation (46)], i.e.

$$\tilde{r} = \int_{\theta=0}^{\pi/2} R(\theta) \sin 2\theta \, d\theta \quad \text{and} \quad \tilde{t} = \int_{\theta=0}^{\pi/2} T(\theta) \sin 2\theta \, d\theta \tag{69}$$

where $R(\theta)$ and $T(\theta)$ are given in equation (63) or, if polarization is ignored, in equation (68). In the case of the nonabsorbing plate of refractive index of 1.5, the difference between the models with and without account for polarization is 4% for the Lambertian reflectance, and less than 1% for the Lambertian transmittance. This can justify that polarization is ignored for transmission filters in applications where no much accuracy is needed, for example in the color assessment of stained glasses or filtered lightings.

6. SURFACE SCATTERING

Compared to a flat interface, a rough interface reflects and transmits collimated incident light into an enlarged set of directions. The topography of the rough interface has a random elevation as featured in Figure 21. The elevation function is modeled by a probability distribution parameterized by a characteristic vertical length, the *root-mean-square (r.m.s.) height* σ, and by a characteristic horizontal length, the *correlation length* τ [8]. Another parameter is also commonly used: the *r.m.s. slope m*, corresponding to the ratio σ/τ [42].
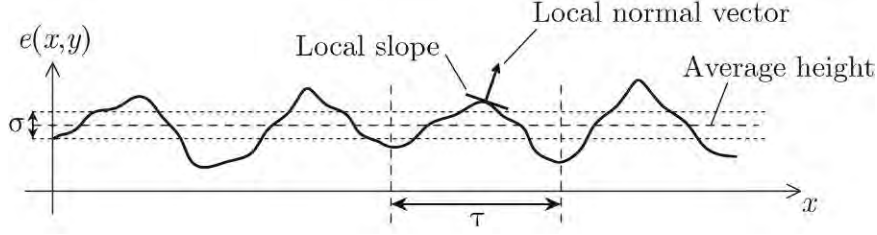
Figure 21. Profile of the elevation function *e* of a rough interface along the *x*-axis. The random pattern has a r.m.s. height σ and a correlation length τ. The r.m.s. slope *m* of the interface is the ratio σ/τ.

Most models assume that the local slope within rough interfaces follows a Gaussian distribution [43, 8]. In order to ease the application of optical laws, local slope is converted into local normal vector [44] denoted by the differential solid angle $d\omega_h = \sin\theta_h d\theta_h d\phi_h$ (Figure 22). For an isotropic Gaussian distribution of slopes, the probability distribution function *D* of the normal vector orientations is

$$D\left(d\omega_h\right) = \frac{e^{-\tan^2\theta_h / 2m^2}}{2\pi m^2 \cos^3\left(\theta_h\right)} \tag{70}$$

This function is known as the *Beckmann function* [8,45,46]. It depends only on the polar angle θ_h due to the assumption of roughness azimuthal isotropy.
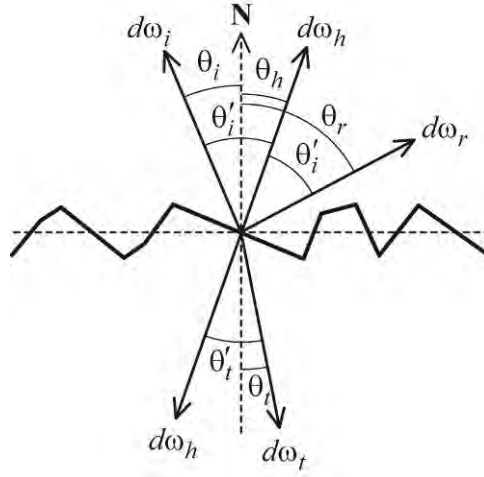
Figure 22. 2D representation of a rough interface. The directional incident light (direction denoted by the differential solid angle $d\omega_i$) hits a small portion of interface having the normal vector $d\omega_h$. It is reflected and transmitted into directions $d\omega_r$ and $d\omega_t$ respectively.

6.1. Bi-directional reflectance and transmittance models

The reflectance and transmittance of rough interfaces can be deduced from their BRDF, respectively their BTDF using equation (21). BRDFs and BTDFs may be determined

experimentally [47,48,8] or computed thanks to an optical model. The model is derived from equations relying on either physical or geometrical optics depending on the size of the roughness patterns [46].

Physical optics models are directly based on the electromagnetic wave theory and Maxwell's equations [2]. They shall be used when the wavelength of light is large or comparable to the r.m.s. height σ and the correlation length τ. In such a case, the diffraction of the incident waves by the corrugations of the interface is dominant. It is assumed that the interface does not have any discontinuity or sharp arc compared to the wavelength of incident light. It may therefore be represented locally by its tangent plane, on which light is reflected according to Snell's law and diffracted because of the small size of the plane. This *tangent plane approximation* is the basis of Beckmann's model [43], also known as *Kirchhoff's approximation* [49].

Models relying on geometrical optics models explain the behavior of light when its wavelength is small compared to the roughness characteristic lengths. Diffraction becomes negligible. *Slope distribution models*, such as the well-known models developed by Torrance and Sparrow [42] and by Cook and Torrance [45] consider the rough interface as a set of randomly inclined microfacets reflecting and transmitting light like flat interfaces. According to slope distributions models [42, 45, 46], the BRDF f_R of a rough interface is

$$f_R\left(d\omega_i, d\omega_r\right) = \frac{D\left(\theta_h\right)G\left(\theta_i, \theta_r\right)R_{12}\left(\theta_i'\right)}{4\cos\theta_i\cos\theta_r} \tag{71}$$

When the medium of transmission is non-metallic, the BTDF is [50]

$$f_T\left(d\omega_i, d\omega_t\right) = \frac{D\left(\theta_h\right)G\left(\theta_i, \theta_t\right)T_{12}\left(\theta_i'\right)}{\Gamma\left(\theta_i'\right)\cos\theta_i\cos\theta_r} \tag{72}$$

In Eqs. (71) and (72), differential solid angles $d\omega_i = \sin\theta_i d\theta_i d\phi_i$, $d\omega_r = \sin\theta_r d\theta_r d\phi_r$ and $d\omega_t = \sin\theta_t d\theta_t d\phi_t$ denote respectively the directions of incidence, of reflection and of transmission (see Figure 22), angle θ_h represents the inclination of the interface's local normal vector, which is related to the angles of incidence and reflection by

$$\theta_h = \arccos\left[\left(\cos\theta_i + \cos\theta_r\right)/\sqrt{2\left(1 + \cos\theta_i\cos\theta_r + \sin\theta_r\sin\theta_i\cos\left(\phi_r - \phi_i\right)\right)}\right], \tag{73}$$

angle θ_i' denotes the local angle of incidence of light, which is related to the angles of incidence and reflection by

$$\theta_i' = \frac{1}{2}\arccos\left(\cos\theta_r\cos\theta_i - \sin\theta_r\sin\theta_i\cos\left(\phi_r - \phi_i\right)\right), \tag{74}$$

function D is the probability distribution function of the local normal vector, given by equation (70), function G is a shadowing function that is presented below, R_{12} is the Fresnel angular reflectance of the interface and $\Gamma\left(\theta_i'\right)$ expresses the spreading of the transmitted solid angle due to the refraction by the interface:

$$\Gamma\left(\theta_i'\right) = \frac{\left(\cos\theta_i' - \sqrt{n^2 - 1 + \cos\theta_i'}\right)^2}{n\cos\theta_i'\sqrt{n^2 - 1 + \cos\theta_i'}} \tag{75}$$

A rough interface may comprise shadow areas, which increase with the roughness and the incidence angle of light. Interface elements belonging to shadow areas do not contribute to the reflection nor the transmission. This phenomenon, illustrated by Figure 23, is called *shadowing*.
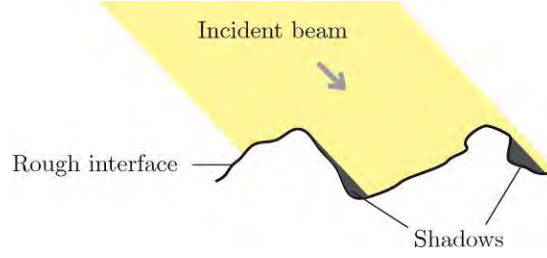

Figure 23. Shadowing: oblique incident light does not illuminate the whole surface.

Likewise, reflected and transmitted light may be partially blocked by neighboring corrugations. This phenomenon, sometimes called *masking* [42], is equivalent to shadowing but depends on the angle of observation instead of the angle of incidence.

The fraction of facets that really contributes to the reflection of light from direction $d\omega_i$ to direction $d\omega_r$ is given by function $G\left(\theta_i, \theta_r\right)$, product of two similar functions g, one for shadowing, and the other one for masking

$$G\left(\theta_i, \theta_r\right) = g\left(\theta_i\right) g\left(\theta_r\right) \tag{76}$$

Using a statistical model, Smith computed the following shadowing function g [51]

$$g\left(\theta, \theta_i'\right) = \begin{cases} \dfrac{1}{\Lambda_m\left(\theta\right) + 1} & \left(\text{if } \cos\theta_i' > 0\right) \\ 0 & \left(\text{if } \cos\theta_i' < 0\right) \end{cases} \tag{77}$$

where θ_i' is the local angle of incidence given by (74) and Λ_m is a function of angle θ which depends on the r.m.s. slope m:

$$\Lambda_m\left(\theta\right) = \frac{1}{2}\left[\frac{1}{\sqrt{\pi}} \cdot \frac{\sqrt{2}m}{\cot\theta}\exp\left(\frac{-\cot^2\theta}{2m^2}\right) - \text{erfc}\left(\frac{\cot\theta}{\sqrt{2}m}\right)\right]$$

Function g is comprised between 0 (facets completely shadowed or masked) and 1 (facets completely illuminated). At small and medium incidence angles, the illuminated fraction of the facet's area is close to 1. The shadowing effect is thus small enough to be neglected. However, ignoring the shadowing at high incidence angles may yield an overestimation of the reflected and transmitted fluxes, and a subsequent violation of the energy conservation principle. According to

Bruce [52] and Caron [53], shadowing should be taken into account when the incidence angle is higher than a limit angle θ_{shad} depending on the r.m.s. slope m of the rough interface

$$\theta_{shad} = \frac{\pi}{2} - \arctan\left(\sqrt{2}m\right) \qquad (78)$$

The same considerations apply for masking.

6.2. Gloss

The light component reflected at the surface of the objects is generally well distinguishable from the component having entered the objects' material. It gives rise to a different perceptual attribute called *glossiness*. This surface reflection component is not or little colored in comparison to the light issued from the matter which is subject to wavelength-dependent absorption. Moreover, the angular distribution of the two components may be very different, especially when the object is diffusing and its surface is smooth or polished.

The study of gloss perception is more recent than the study of color [54] and yet there is no normalized gloss perception space available today. The main approach consists at correlating gloss perception, surface topology and BRDF measurements [55], but in the case of colored objects, it is still difficult to assess color and gloss attributes from optical measurement [28]. First attempts of gloss assessment are due to Hunter, Judd and Wyszecki [56] but according to Wills, Agarwal, Kriegman and Belongie [57], the modern notion of gloss was formalized by the American Society for Testing and Materials (ASTM) as "the angular selectivity of reflectance, involving surface-reflected light, responsible for the degree to which reflected highlights or images of objects may be seen as superimposed on a surface" [58]. In order to cope with the variety of materials and gloss effects, several types of glossiness are defined, each one being assess by measurement with a specific $\theta_i{:}\theta_r$ bidirectional geometry [20]: *specular gloss* is the perceived brightness associated with the specular reflection from a surface (measurement geometries: 20°:20°, 45°:45° and 60°:60°), *sheen* is the perceived shininess from matte surfaces at grazing angles (85°:85°), *Distinctness of image (DOI)* is the perceived sharpness of images reflected in a surface (30°:30.3°). *Bloom*, also *called 2∘ Haze*, is the perceived cloudiness in reflections near the specular direction (30°:32°), *Haze* is the shininess measured at 5° to the specular direction (30°:35°), *diffuseness* is the perceived brightness for diffusely reflecting areas (30°:45°) and *contrast gloss* is the perceived relative brightness of specularly and diffusely reflecting areas (45°:45° and 45°:0° geometries).

7. VOLUME SCATTERING

As light encounters small fluctuations of refractive index within the medium, a portion of the incident light is scattered. In the atmosphere, scattering yields the white color of clouds (Mie

scattering [59]), the blue color of the sky and the redness of sunsets (Rayleigh scattering [60]). Scattering also occurs in liquids. Milk, for example, is composed of a suspension of almost transparent fat droplets which scatter light and give milk its white and opaque aspect. In the case of oceans, scattering is coupled to absorption, which produces the characteristic bluish color. Light is also scattered in solid heterogeneous media, such as paintings, papers, cotton and human tissues [61]. Different types of scattering are encountered according to the composition, shape, size and concentration of the heterogeneities, often considered as particles immerged into a binder. The polarization and the wavelength of the incident light may have a strong influence on scattering. We present here some commonly used parameters and models relative to scattering.

7.1. Scattering description parameters

A collimated beam traversing a path of length x into a scattering and absorbing medium undergoes an exponential attenuation T described by the Beer-Lambert law

$$T = e^{-K_{ext}x} \tag{79}$$

where K_{ext} is the *linear extinction coefficient* (in m^{-1}). The inverse of the extinction coefficient is the *extinction mean-free-path length* l_{ext}, characterizing the distance along which directional flux is attenuated by a factor $1/e$

$$l_{ext} = 1/K_{ext} \tag{80}$$

The linear extinction coefficient may be decomposed into a component K_{sca} related to scattering and a component K_{abs} related to absorption

$$K_{ext} = K_{sca} + K_{abs} \tag{81}$$

Mean-free-path lengths are also defined for scattering l_{sca} and for absorption l_{abs}

$$l_{sca} = 1/K_{sca} \text{ and } l_{abs} = 1/K_{abs} \tag{82}$$

The scattering and absorbing medium is said to be *homogenous* when its coefficients K_{sca} and K_{abs} are independent of position. These coefficients are generally functions of wavelength. Beer's law corresponds to the special case where $K_{sca} = 0$.

As an effect of scattering, the trajectory of light is modified. The change of direction in an elementary volume of medium is specified by a *volume angular scattering coefficient* (VSF) [7], defined for every direction (θ, φ) as

$$\beta_\lambda(\theta, \varphi) = \frac{d^2\Phi_\lambda(\theta, \varphi)}{E_\lambda d\omega dV} = \frac{dI_\lambda(\theta, \varphi)}{E_\lambda dV} \tag{83}$$

where $d^2\Phi_\lambda$ denotes the element of spectral flux scattered out of the volume dV into the elemental solid angle $d\omega$, E_λ the incident collimated spectral irradiance and $dI_\lambda = d^2\Phi_\lambda / d\omega$ the scattered element of spectral intensity. The VSF integrated over the 4π sr solid angle gives the

linear scattering coefficient $K_{sca}(\lambda)$. Hence, dividing the VSF $\beta_\lambda(\theta,\phi)$ by $K_{sca}(\lambda)$ yields a normalized function called *angular scattering distribution function* $f_S(\lambda,\theta,\phi)$ satisfying the following normalization condition for each wavelength

$$\int_{(\theta,\phi)\in 4\pi} f_S(\lambda,\theta,\phi)\, d\omega = 1 \tag{84}$$

Even though f_S is independent of absorption, it remains a function of wavelength as directions of scattering generally depend upon wavelength especially when scattering is due to diffraction (Rayleigh scattering, Mie scattering [2]). The rigorous definition for f_S is the ratio of scattered element of intensity $dI_\lambda = d^2\Phi_\lambda/d\omega$ to total scattered element of flux $d\Phi_\lambda$

$$f_S(\lambda,\theta,\phi) = \frac{dI_\lambda(\theta,\phi)}{d\Phi_\lambda} \tag{85}$$

Equation (84) comes from the fact that the total scattered spectral flux $d\Phi_\lambda$ is the sum of all spectral intensities over the 4π sr solid angle. If scattering by the volume element is isotropic, equal intensity is emitted in every direction and function f_S is a constant equal to $1/4\pi$. The ratio of the function f_S of a given medium to the one of an isotropic diffuser is called the *phase function*, denoted as *P*:

$$P(\lambda,\theta,\phi) = 4\pi\, f_S(\lambda,\theta,\phi) \tag{86}$$
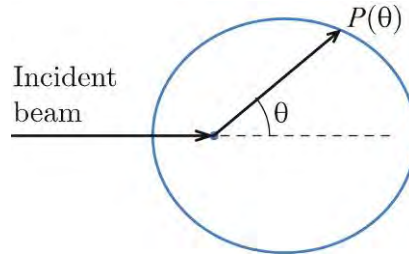
Figure 24. Example of phase function of a scattering medium in the plane $\phi = 0$ for one wavelength.

Figure 24 shows an example of phase function represented in one plane containing the incident beam. As a consequence of equations (84) and (86), the normalization equation for the phase function is

$$\frac{1}{4\pi}\int_{(\theta,\phi)\in 4\pi} P(\theta,\phi)\, d\omega = 1 \tag{87}$$

In the case of isotropic scattering, the phase function is 1 in all directions. In the opposite case, anisotropic scattering may be characterized by an *anisotropy parameter g* defined as the average cosine of the scattering angle

$$g = \frac{1}{4\pi} \int_{(\theta,\varphi)\in 4\pi} P(\theta,\varphi)\cos\theta d\omega = 1 \qquad (88)$$

The incident light is mainly scattered backwards when g is close to –1 or forwards when g is close to 1. For isotropic scatterings, $g = 0$. Parameter g is used for defining the *transport mean-free-path length l_{trans}*, corresponding to the distance from which one may consider that light has completely lost the memory of its original direction of incidence

$$l_{trans} = \frac{l_{sca}}{1-|g|} \qquad (89)$$

The *optical thickness* τ of a scattering or/and absorbing layer having a thickness h and an extinction coefficient K_{ext} is defined as

$$\tau = K_{ext}h \qquad (90)$$

When $\tau \gg 1$, a directional incident light is almost completely attenuated. When τ is small, the layer is translucid, i.e. we can distinguish an object located beneath the layer. After a certain number of scattering events, light propagates in an isotropic manner, i.e. it becomes Lambertian.

7.2. Types of scattering

The notion of optical thickness defined above allows estimating the number of scattering events that a light ray undergoes across a given layer of the considered medium. In the particular case of a weakly absorbing medium ($K_{abs} \ll K_{sca}$), the optical thickness describes the strength of scattering. We may distinguish four scattering modes, according to the value of the optical thickness of the layer:

− *ballistic scattering*, also called *atmospheric absorption* [6], in which light is almost not scattered: $\tau \ll 1$ and $h \ll l_{sca}$,

− *single scattering* in which light is scattered once in the medium: $\tau \approx 1$ and $h \approx l_{sca}$. For particle sizes much smaller than the wavelength such as air molecules, smoke and dust, Rayleigh scattering [41, 60, 62] is applicable with the following phase function for unpolarized light:

$$P_R(\theta,\varphi) = \frac{3}{8}\left(1+\cos^2\theta\right) \qquad (91)$$

For larger particles with size comparable to the wavelength, Mie scattering [59, 202] becomes applicable and is often represented by approximated phase functions such as the famous Henyey-Greenstein phase function [63] parameterized by the anisotropy parameter g defined in equation (88)

$$P_{HG}(\theta,\varphi) = \frac{1-g^2}{\left(1-2g\cos\theta+g^2\right)^{3/2}} \qquad (92)$$

When particle sizes are much larger that the wavelength, geometrical optics models may be used [64, 65].

− *multiple scattering* in which light is scattered various times [66]: $\tau > 1$ and $h > l_{sca}$,

− *diffusion* where scattering events occur so many times that the resulting scattering is isotropic: $\tau \gg 1$ and $h \gg l_{sca}$. According to Eq. (90), since parameter g defined by (88) is equal to 0, the transport length is given by the scattering length. The incident light has therefore completely lost the memory of its incident direction.

For low concentrations of particles, it is assumed that they do not interact with each other. Scattering is said to be *independent*. Describing the scattering by one particle is sufficient to determine the scattering by the whole medium. For high concentrations of particles, scattering becomes *dependent*. In the case of independence, geometrical optics may be used when the size of the particles are large compared to the wavelength of the incident light. However, when the particles are small compared to the wavelength, light is diffracted. In this case, scattering may be modeled by the Rayleigh scattering theory. The Mie scattering theory describes the diffraction of light by spherical particles of complex refractive index in a dielectric medium (real refractive index). Note that except for exceptional phenomena such as the Raman effect, scattering does not modify the wavelength of the incident light and is thus said to be *elastic* [36].

7.3. The radiative transfer equation

In many applications, a simple phenomenological approach, based on the notion of directed light ray and conservation of energy, provides a realistic description of the scattering phenomenon. Considering a sufficiently large portion of the heterogeneous medium, the scattering process is described by a simple equation: the *radiative transfer equation* [67]. It is valid only when the scattering mean-free-path length l_{sca} is large compared to the wavelength of the incident light and to the dimension of the heterogeneities responsible for the scattering, but specific studies have shown that its domain of validity can be enlarged to other cases.

The radiative transfer equation expresses the conservation of the radiant flux in a given element of volume and a given direction. This energy balance shall be performed everywhere in the medium and in every direction. Let us consider a small cylinder of section dS and of length dl oriented according to the incident direction **u**. Radiance $L(\mathbf{u})$ decreases along this direction due to absorption and scattering

$$\frac{dL(\mathbf{u})}{dl} \propto -\left(K_{abs} + K_{sca} \right) L(\mathbf{u}) \tag{93}$$

At the same time, the cylinder receives radiances $L(\mathbf{u}')$ from all directions $\mathbf{u}'$ and scatters them partially towards direction **u**, which increases radiance $L(\mathbf{u})$. The portion of radiance $L(\mathbf{u}')$ that contributes to radiance $L(\mathbf{u})$ is $\frac{K_{sca}}{4\pi} P(\mathbf{u}',\mathbf{u}) L(\mathbf{u}') d\omega'$, where $P(\mathbf{u}',\mathbf{u})$ is the phase function of

the considered cylindrical element of volume. By summing up the contributions of all directions **u′** and adding the resulting global contribution to equation (93), one obtains the radiative transfer equation

$$\frac{dL(\mathbf{u})}{dl} = -\left(K_{abs} + K_{sca}\right) L(\mathbf{u}) + \frac{K_{sca}}{4\pi} \int_{\Sigma} P(\mathbf{u}', \mathbf{u}) L(\mathbf{u}') \, d\omega' \qquad (94)$$

This equation has no general solution. An exact or approximated solution must be searched for every particular scattering medium. Various solutions have been developed. Let us mention the major ones:

− The *N*-fluxes method [68], which allows converting the integrodifferential equation (94) into a differential equation system thanks to an angular discretization. Solutions are obtained for azimuthally isotropic media, the discretization being performed only according to the zenithal angle [69]; the simplest particular case is the two-flux Kubelka-Munk model [70, 71]. Four-flux models have also been developed [72, 73].

− The discrete ordinate method [74], which is an exact but computationally expensive method. The assumption of azimuthal isotropy is not necessary. Discretization according to the azimuthal angle is avoided thanks to a Fourier series development for the scattered fluxes and a spherical harmonic decomposition of the phase function.

− The auxiliary function method [75], which avoids angular discretization. An auxiliary function is introduced into the radiative transfer equation and decomposed into spherical harmonics. The radiative transfer equation is thus converted into an integral equation system, which can be solved numerically.

− The adding-doubling method [76, 61] is based on an infinitesimal sublayer whose optical properties are described by a matrix. The (*i,j*)-entries of the matrix, deduced from the phase function, indicate the probability for a ray coming from direction *i* to be scattered into direction *j*. Then, the matrix is squared, or raised to a power *k*, to represent the optical properties of a sublayer with double thickness, respectively with thickness multiplied by *k*. This "doubling" or "adding" operation is repeated until the thickness of the sublayer match the whole considered layer thickness.

7.4. Scattering in Lambertian layers

The mean-free-path length l_{sca} of a strongly scattering layer is very small compared to the layer thickness. Incident light looses the memory of its initial angular distribution as soon as it penetrates the layer. We can therefore assume that any illumination geometry leads to a same reflectance and a same transmittance, called *intrinsic*. Since light is scattered a large number of times within the layer, it is Lambertian at every point of the layer, especially at the layer's bounding planes. We can also assume that light exiting the layer is unpolarized.

The reflection and transmission by Lambertian layers can be modeled by the Kubelka-Munk two flux model [70, 71], with a satisfying accuracy if the layer is weakly absorbing [69, 77].

8. THE KUBELKA-MUNK MODEL

The scattering model proposed by Kubelka and Munk [70, 71] was initially introduced for predicting the reflectance of paints, but it has been also used in a wide range of domains where uniform and infinitely large layers of a scattering medium are encountered. It corresponds to a special case of the radiative transfer theory where the phase function is reduced to a pair of opposite directions or, more precisely, of opposite sets of directions covering respectively the upper and the lower hemispheres [78]. It is thus often qualified as a "two-flux model". The interest of the Kubelka-Munk model lies in the simple differential equation system expressing the scattering and absorption phenomena within the layer. The differential equations involve the upward and the downward oriented fluxes, which are functions of depth in the layer. Another interest of this model is the fact that the solutions of the differential equation system have analytical expression.

8.1. Kubelka-Munk differential equation system

The Kubelka-Munk model considers a thin slice of material whose thickness dz is small compared to its two other dimensions (see Fig. 25). Let us denote as j a diffuse flux oriented upwards and as i a diffuse flux oriented downwards. We assume that all variations of fluxes are due to absorption and scattering. Let us denote K the linear absorption coefficient and S the linear scattering coefficient.

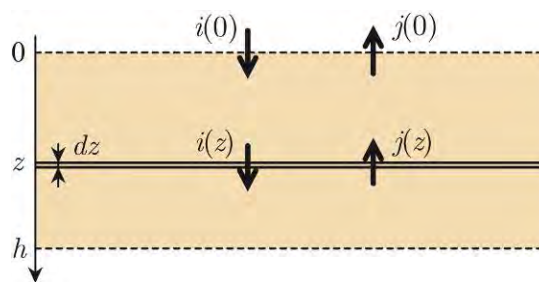Fig. 25. Upward and downward diffuse fluxes crossing a sublayer of thickness dz.

By crossing the slice of matter, the flux $i(z)$ decreases by an amount $(Kdz)i(z)$ due to absorption and also by an amount $(Sdz)i(z)$ due to scattering. However, it increases by the amount of flux $j(z)$ lost by scattering while crossing the same slice of material in the opposite direction: $(Sdz)j(z)$. Therefore we get:

$$\frac{di}{dz} = -(K+S)i + Sj \tag{95}$$

Analyzing the flux j leads to a similar equation. The orientation of this flux being opposite, we need to introduce negative signs:

$$\frac{dj}{dz} = (K+S)j - Si \tag{96}$$

Combining equations (95) and (96) gives a system of differential equations:

$$\begin{cases} \dfrac{di}{dz} = -(K+S)i + Sj \\[2mm] \dfrac{dj}{dz} = -Si + (K+S)j \end{cases} \tag{97}$$

8.2. Solving the differential equation system

There are several ways to solve equation (97), we will present two approaches. The first one uses the Laplace transform and the second one uses the matrix exponential. The Laplace transform [79] associates to a causal function $f(x)$ the function $F(p)$ such that

$$F(p) = \int_0^\infty f(t)e^{-pt}dt \tag{98}$$

It is a linear transform. The derivative of a function f is transformed into $pF(p) - f(0)$, where the constant $f(0)$ is the value of f at $x = 0$. Considering the Laplace transform of Eq. (97), we get the following system:

$$\begin{cases} pI(p) - i(0) = -(K+S)I(p) + SJ(p) \\ pJ(p) - j(0) = SI(p) - (K+S)J(p) \end{cases} \tag{99}$$

where $I(p)$ and $J(p)$ are the Laplace transforms of $i(z)$ and $j(z)$ respectively. Solving Eq. (99) yields:

$$\begin{cases} I(p) = \dfrac{(p - a\,S)i(0) + Sj(0)}{p^2 - b^2 S^2} \\[4mm] J(p) = \dfrac{(p + aS)j(0) - Si(0)}{p^2 - b^2 S^2} \end{cases} \tag{100}$$

with

$$a = (K+S)/S \quad \text{and} \quad b = \sqrt{a^2 - 1} \tag{101}$$

When a function has a Laplace transform, this latter is unique. The converse is also true. Since $p/(p^2 - b^2 S^2)$ and $bS/(p^2 - b^2 S^2)$ are the respective Laplace transforms of $\cosh(bSz)$ and $\sinh(bSz)$ [80], one concludes that $I(p)$ and $J(p)$ are the respective Laplace transforms of

$$i(z) = i(0)\cosh(bSz) + \frac{1}{b}\left[j(0) - ai(0)\right]\sinh(bSz) \tag{102}$$

and

$$j(x) = j(0)\cosh(bSx) + \frac{1}{b}\left(aj(0) - i(0)\right)\sinh(bSx) \tag{103}$$

Expressions (103) and (102) are the general solutions of the Kubelka-Munk differential equation system.

The second approach looks at equation (97) as a differential equation in a vector space that can be written as

$$\frac{d}{dz}\begin{pmatrix} j \\ i \end{pmatrix} = \begin{pmatrix} -(K+S) & S \\ -S & (K+S) \end{pmatrix} \cdot \begin{pmatrix} j \\ i \end{pmatrix} \tag{104}$$

The solution of this Eq. is given by the matrix exponential of the matrix [81]:

$$\begin{pmatrix} j(z) \\ i(z) \end{pmatrix} = \exp\left[\begin{pmatrix} -(K+S) & S \\ -S & (K+S) \end{pmatrix}(z-0)\right] \cdot \begin{pmatrix} j(0) \\ i(0) \end{pmatrix} \tag{105}$$

where the matrix exponential is defined by similar series as the classical exponential:

$$\exp(\mathbf{M}) = \sum_{k=0}^{\infty} \frac{\mathbf{M}^k}{k!} = \mathbf{I} + \mathbf{M} + \frac{\mathbf{M}^2}{2} + \frac{\mathbf{M}^3}{6} + \frac{\mathbf{M}^4}{24}\dots \tag{106}$$

Let us now derive the reflectance and transmittance of a layer of thickness h considered without interface. Denoting as I_0 incident flux on the front side, the layer's reflectance and transmittance correspond to the flux ratios $j(0)/I_0$, respectively $i(h)/I_0$. As boundary conditions, we have:

$$i(0) = I_0 \tag{107}$$

and

$$j(h) = 0 \tag{108}$$

By setting these boundary conditions in equations (102) and (103), or equivalently into Eq. (105), at depth $z = h$, we obtain the following reflectance and transmittance formulas

$$\rho_h = \frac{j(0)}{I_0} = \frac{\sinh(bSh)}{b\cosh(bSh) + a\sinh(bSh)} \tag{109}$$

and

$$\tau_h = \frac{i(h)}{I_0} = \frac{b}{b\cosh(bSh) + a\sinh(bSh)} \tag{110}$$

with a and b given in Eq. (101).

8.3. Infinitely thick layer

Let us consider the particular case of a layer whose thickness becomes infinite. From Eq. (110), we can compute the limit as shown in Eq. (111)

$$\lim_{h \to \infty} \rho_h = \lim_{h \to \infty} \frac{1}{a + b \coth(bSh)} = \frac{1}{a+b} = a - b \tag{111}$$

Let us denote this limit as ρ_∞. In literature (see Ref. [18], p.785), ρ_∞ is expressed as a function of K and S

$$\rho_\infty = 1 + \frac{K}{S} - \sqrt{\left(\frac{K}{S}\right)^2 + 2\frac{K}{S}} \tag{112}$$

The ratio between K and S can be expressed as a function of ρ_∞

$$\frac{K}{S} = \frac{(1-\rho_\infty)^2}{2\rho_\infty} \tag{113}$$

Eq. (113) is the most popular result from the Kubelka-Munk theory.

An observer perceives a layer of finite thickness h as "infinitely thick" if no light emerges on the other side. In practical terms this is an opaque layer and yields the boundary condition $i(h) = 0$. Combined with the boundary conditions expressed in equations (107) and (108), Eq. (102) becomes

$$I_0 \cosh(bSh) + \frac{j(0) - aI_0 \sinh(bSh)}{b} = 0 \tag{114}$$

thus providing

$$\rho_\infty = a \sinh(bSh) - b \cosh(bSh)$$

8.4. Layer in optical contact with a background

Many practical cases, like ink on paper or paint on a substrate, can be seen as layers in optical contact with a background having a reflectance factor ρ_g. Now the boundary condition at $x = h$ are given by

$$j(h) = \rho_g i(h) \tag{115}$$

Substituting equations (115) and (107) in equations (102) and (103) leads to:

$$\rho = \frac{(1 - a\rho_g)\sinh(bSh) + b\rho_g \cosh(bSh)}{(a - \rho_g)\sinh(bSh) + b\cosh(bSh)} \tag{116}$$

Assuming $bSh \neq 0$, Eq. (116) can be simplified as:

$$\rho = \frac{1 - \rho_g(a - b\coth(bsh))}{a - \rho_g + b\coth(bSh)} \tag{117}$$

Equation (117) is called the *hyperbolic solution* of the Kubelka-Munk equations. As bSh tends to 0, ρ tends towards ρ_g.

Two particular cases of interest are the reflectances ρ_0 and ρ_1 of a layer in optical contact with an ideal black background and an ideal white background, respectively:

$$\rho_0 = \frac{\sinh(bSh)}{a\sinh(bSh) + b\cosh(bSh)} \tag{118}$$

and

$$\rho_1 = \frac{(1-a)\sinh(bSh) + b\cosh(bSh)}{(a-1)\sinh(bSh) + b\cosh(bSh)} \tag{119}$$

8.5. Saunderson correction

The reflectances modeled by the previous equations do not take into account the reflections of light at the interface with air, whereas these reflections are significant and cannot be ignored. Saunderson proposed a correction for the Kubelka-Munk reflectance formula taking them into account [82].

Let us denote as R the effective reflectance of the layer and ρ the reflectance it would have without interface given by the Kubelka-Munk model. Reflectance ρ is defined as the ratio of upward to downward fluxes at depth 0, i.e. $\rho = j(0)/i(0)$. The effective reflectance is the ratio of outgoing to incoming fluxes, i.e. $R = J_0/I_0$. Regarding the flux coming from air, a fraction r_e of it (external reflectance) is reflected and a fraction T_{in} is transmitted into the medium (see Figure 26). Regarding the upward flux $j(0)$ coming from the medium, a fraction r_i of it (internal reflectance) is reflected and a fraction T_{out} is transmitted to air. We have:

$$\begin{aligned} i(0) &= T_{in}I_0 + r_i\rho i(0) \\ J_0 &= r_e I_0 + T_{out}\rho i(0) \end{aligned} \tag{120}$$
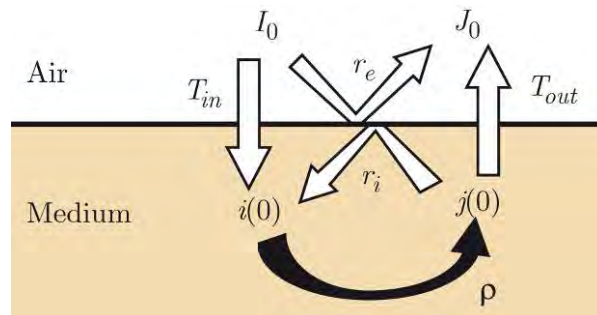

Fig. 26. Reflections and transmissions of diffuse light at the air-medium interface.

From these two equations, we derive the Saunderson correction formula:

$$R = r_e + \frac{T_{in}T_{out}\rho}{1 - r_i\rho} \qquad (121)$$

The terms r_e, r_i, T_{in}, and T_{out} depend only on the refractive index of the medium. Assuming that the interface is flat, they are derived from the Fresnel formula in respect to the illumination and observation geometries.

In the case of a diffuse-diffuse geometry, the incident flux is Lambertian and the whole reflected light is captured by the detector. We thus have: $r_e = r_{12}$ given by Eq. (47), $r_i = r_{21}$ deduced from r_{12} according to Eq. (50), $T_{in} = t_{12} = 1 - r_{12}$ and $T_{out} = t_{21} = 1 - r_{21}$. In the case of diffuse-directional geometry, where the incident light is Lambertian and only the radiance in one direction (at angle θ to the normal) is observed, we rather have: $r_e = R_{01}(\theta)/\pi$ and $T_{out} = T_{01}(\theta)/(n^2\pi)$, where $R_{01}(\theta)$ and $T_{01}(\theta)$ denote the Fresnel angular reflectance, respectively angular transmittance, of the interface. The factors $1/\pi$ come from the fact that the radiance exiting towards the observer forms only a fraction $1/\pi$ of the total incoming fluxes (see Section 3.5), but they remove if one considers the reflectance factor in respect to a perfectly white diffuser. The term $1/n^2$ in T_{out} comes from the changing of solid angle due to the refraction of exiting rays through the interface, as explained in Section 4.5.

8.6. Saunderson correction in transmittance mode

When a layer of diffusing medium is observed by transmission of light, the reflections and transmissions of light at the interfaces may be modeled in a similar manner as in reflectance mode, except that the incident flux I_0 illuminates the back air-medium interface. We denote as ρ and τ the intrinsic reflectance, respectively intrinsic transmittance of the layer, and as r_i and r_i' the internal reflectance of the top interface, respectively the back interface for Lambertian light. The flux transfers represented in Fig. 26 enable writing the following equations:

$$\begin{aligned}
i(0) &= r_i j(0) \\
j(0) &= \rho i(0) + \tau j(h) \\
i(h) &= \rho j(h) + \tau i(0) \\
j(h) &= T_{in}I_0 + r_i'i(h) \\
J_0 &= T_{out}j(0)
\end{aligned} \qquad (122)$$

We deduce the expression for the layer's transmittance with interfaces:

$$T = \frac{J_0}{I_0} = \frac{T_{in}T_{out}\tau}{(1 - r_i\rho)(1 - r_i'\rho) - r_i r_i'\tau^2} \qquad (123)$$

Since the layer is bounded by air at its two sides, the two internal interface reflectances are: $r_i = r_i' = r_{21}$. The terms T_{in} and T_{out} are similar as those presented in the previous section for the reflectance mode.
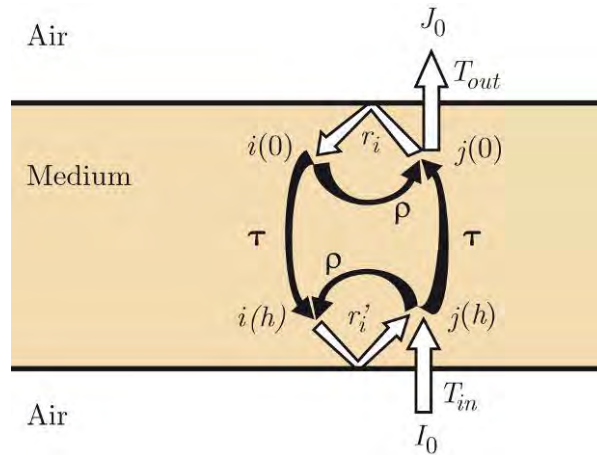
Fig. 27. Reflections and transmissions of diffuse light at the air-medium interfaces in transmittance mode.

8.7. Validity of the Kubelka-Munk model

The Kubelka-Munk model became famous in many technical domains where light scattering is concerned, mainly owing to its reduced number of parameters (absorption coefficient, scattering coefficient and medium thickness) and a set of simple formulas relating these parameters with measurement easily performable in practice. However, in many cases, large deviation between prediction and measurement is observed due to the fact that the medium optical properties and/or the light and measurement conditions are not compatible with the assumptions underlying the model. Abundant literature has been dedicated to the statement of the Kubelka-Munk limitations as well as improvements for specific applications. As a special case of the radiative transfer theory, the Kubelka-Munk model relies on the following assumptions: the average distance between diffuser and/or absorbers should be very large compared to the wavelengths of light. The absorbing and scattering particles should therefore be relatively far from each other in respect to the wavelength of light, as fibers in paper for example. The model assumes Lambertian illumination and is not adapted in case of collimated illumination. It also assumes strong, isotropic scattering in a homogenous semi-infinite medium. It does not apply with media whose scattering and absorption coefficient vary locally at mesoscopic scale, for example halftone ink dots in paper.

The K and S values for which accurate predictions may be expected from the model is often discussed. In many cases, in particular when the concentration in either absorbing particles or scattering particles is increases, the other one remaining constant, one observes that both K and S parameters vary, whereas only one of them should vary [86]. This leads to the conclusion that the two coefficients are interdependent. This is the reason why in many applications one rather consider the K/S ratio, closely related to the reflectance of an infinitely thick medium according to Eq. (113), instead of separate K and S parameters. Lastly, anisotropy of the propagating fluxes is a main concern of the Kubelka-Munk theory. Nobbs [87] noticed that the assumption of uniformly

diffuse flux propagating in opposite directions is valid only for nonabsorbing media, otherwise the fluxes become anisotropic and different absorption and scattering coefficients should be defined for each propagation direction. Anisotropic scattering is modeled by Monte-Carlo simulations or extensions of the Kubelka-Munk theory such as the multi-flux model developed by Mudgett and Richards [68], the four-flux model by Maheu et al. [88], or the ones presented in Chapter [hdi055].

9. FLUORESCENCE

Fluorescent materials are present in nearly every printed item. Paper looks white thanks to fluorescent brighteners embedded within the paper bulk. Fluorescent dyes are present in many different articles, such as paints, crayons, toys, life saving jackets and safety signs. Ink manufacturers sell fluorescent inks used in the graphic arts to create special effects. There is also a high interest for fluorescence in biology and life sciences in order to get information about dynamic processes within living cells.

We first describe the fluorescence phenomenon in a qualitative manner and then show how material fluorescence can be captured directly by measurements or derived from measurements by calculations. These base concepts are useful for example for characterizing under a given illuminant the reflectance and color of paper with fluorescent brighteners or of paper printed with daylight fluorescent inks. We also show how to decompose the total reflectance into a pure reflectance that is independent of the illuminant and into a fluorescent emission that depends strongly on the illuminant. Advanced topics such as models predicting the reflectance of fluorescent ink halftones are outside the scope of the present section.

9.1. The luminescence phenomenon

Luminescence is the phenomenon of light emission by atoms or molecules that have been excited by the absorption of energy from chemical reactions, irradiation by light, electron impact, electrical current, mechanical strains, etc. *Photoluminescence* denotes the luminescence caused by absorption of ultraviolet, visible or infrared radiation. *Fluorescence* is a form of photoluminescence where light is emitted at a wavelength different from the wavelength of the exciting light and where the decay is determined by a time constant in the order of 10^{-8} s.

Fluorescence relies on the *absorption* of photons, on the *transitions* of a molecule from a ground energy state to excited energy states and on the release of the absorbed energy by the *emission of light*, generally at a wavelength longer than the wavelength of absorption. Absorption is a discrete process, where incoming absorbed photons raise the energy of the considered molecule from the ground state E_0 to a certain vibrational level E_{ij} of the excited state E_i, which depends on the

molecular structure of the considered material. Only photons hitting the molecule having the required energy E_p are absorbed:

$$E_p = h\nu = \frac{hc}{\lambda} \qquad (124)$$

This explains why absorption of photons takes place only at certain discrete wavelengths. Since molecules have many energy levels, a typical absorption spectrum consists of multitudes of absorption lines, yielding a nearly continuous absorption spectrum. The left part of Figure 28 shows molecular absorption into the vibrational levels E_{1j} of energy state E_1.

Shortly after absorption, a very fast non-radiative relaxation process brings the different vibrational levels of energy state E_1 back to their lowest vibrational level E_{10}. The average lifetime of the vibrational state is approximately only 10^{-15} s.

From the lowest level of energy state E_1, there is a transition to one of the vibrational states of the ground state E_0 by fluorescent emission. Since there are a finite number of vibrational states, the emitted wavelengths are those which correspond to the energy difference between the lowest energy level E_{10} of excited state E_1 and vibrational levels E_{0j} of the ground state E_0.
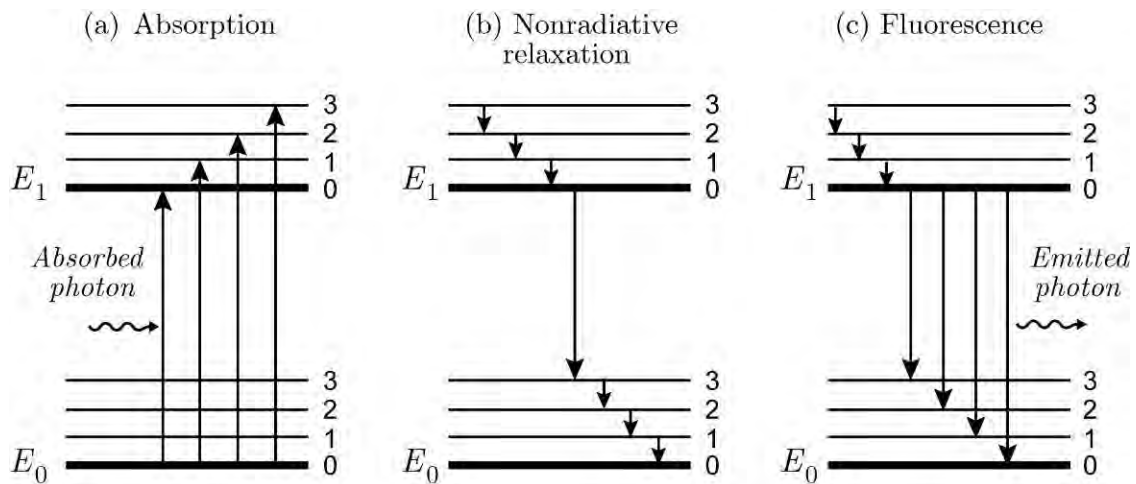

Figure 28. Energy diagram showing the vibrational levels of energy ground state E_0 and excited state E_1, (a) energy absorption, (b) non-radiative relaxation and (c) fluorescent emission.

As shown in Figure 28, in the general case, the absorbed energy differences from the lowest level of ground state E_0 to one of the vibrational levels of the excited state E_1 are larger than the fluorescently emitted energy differences from the lowest level of the excited state E_1 to one of the vibrational levels of the ground state E_0. This explains why the wavelengths of the *fluorescent emission spectrum* are higher than the wavelengths of the *absorption spectrum*. This shift to larger wavelengths is called the *Stokes shift* [89].

Figure 28 also shows that fluorescence takes always place from the lowest energy level of excited state E_1 to the different vibrational levels of ground state E_0. Therefore, for a single species, its emission wavelengths do not depend upon the excitation wavelengths. This means that the shape of the fluorescent emission spectrum is the same, independently of the spectral power distribution of the exciting illuminant. However, the intensity of the fluorescent emission spectrum depends upon the power distribution and intensity of the exciting illuminant.

9.2. Characterizing and measuring the fluorescence

Fluorescence is only one of several relaxation mechanisms by which a molecule returns to its ground state after having been excited by absorption of radiation. Often, non-radiative relaxation and fluorescence occur simultaneously. Fluorescence of a substance is partly characterized by the shape of its emission spectrum. Globally, the *quantum yield* defined as the ratio of the number of emitted photons to the number of absorbed photons per unit of time characterizes the fluorescence potential of a substance.

Different absorption wavelengths may induce more or less fluorescence. If a material absorbs q_0 photons per unit time at an excitation wavelength λ and reemits a total of q photons per unit time within the entire emission band, the *quantum efficiency Q_e* of the material at wavelength μ is defined as

$$Q_e(\lambda) = q / q_0(\lambda) \tag{125}$$

It has been shown that for some materials, the quantum efficiency is nearly constant over a large number of excitation wavelengths [Donaldson 1954]. Nevertheless, in the general case, the power distribution of the excitation illuminant has a strong impact on the resulting emission spectrum intensity.

The fluorescence of a substance can be characterized independently of the excitation illuminant by establishing the Donaldson fluorescence matrix [84], whose entries give the percentage of light emitted by fluorescence or reflected by pure reflectance at successive discrete wavelengths of the emission spectrum (rows) when illuminated only at a specific discrete wavelength (column). These entries are usually given in terms of ratios of radiant energy. The Donaldson fluorescence matrix $\mathbf{F}$ has the structure given in Figure 29. Its entries F_{ij} indicate the ratio of exiting energy at wavelength i to the excitation energy at wavelength j.

The values on the diagonal F_{ij} of fluorescence matrix $\mathbf{F}$ represent the pure reflectance at wavelength i. The values F_{ij} with $i > j$ represent the radiant (energy) efficiency, i.e. the ratio between excitation energy at wavelength j and emission energy at wavelength i. In classical fluorescent media with a positive Stokes shift, the entries F_{ij} with $i < j$ are zero.

	Excitation wavelength range			
λ (nm)	300	310	...	730
300	$F_{0,0}$	$F_{0,1}$		$F_{0,43}$
310	$F_{1,0}$	$F_{1,1}$		$F_{1,43}$
...				
730	$F_{43,0}$	$F_{43,1}$		$F_{43,43}$

Figure 29. Example of Donaldson matrix **F** for wavelengths between 300 and 730 nm.

By multiplying the fluorescence matrix **F** with the excitation irradiance vector **I**, one obtains the output irradiance **E** comprising both the purely reflected and the irradiance components emitted by fluorescence

$$\mathbf{E} = \mathbf{F} \cdot \mathbf{I}, \qquad (126)$$

where in our example **E** and **I** are vertical vectors comprising respectively the irradiance components $E_0 E_1, .. E_{43}$ and $I_0 I_1, .. I_{43}$ and where matrix **F** is the matrix shown in Figure 29.

The entries of the Donaldson fluorescence matrix can be experimentally acquired by a spectrofluorimeter or a double monochromator device. Such a device decomposes the incident light into narrow wavelength bands which are successively selected to illuminate the sample. The light emitted and reflected by the sample is captured into a spectrometer which decomposes it into narrow wavelength bands, expressed by components E_i of vector **E**. Fluorescence spectrometers relying on monochromators or narrow band filters for single wavelength narrow band light emission and on spectrometers for the spectral decomposition and acquisition of the emitted and reflected light need to be carefully calibrated. They must account for the following elements: power distribution of the light source, wavelength-dependent light attenuation variations by the monochromator or the narrow band filters, wavelength-dependence of the capturing optics and fibers and wavelength-dependent sensibility of the spectrometer.

9.3. Total reflectance and pure reflectance of fluorescent samples

Fluorescent print reflection models often rely on the superposition paradigm: light apparently reflected by a sample formed by a fluorescent layer on a diffusing substrate (e.g. a print) is the light reflected by that sample without fluorescence plus the light emitted by fluorescence. Often it is possible to separate the excitation wavelength range from the emission wavelength range. For example, paper with fluorescent additives is excited in the near UV wavelength range and emits in the blue wavelength range.

In the case that the excitation wavelength range is lower than the emission wavelength range (which is generally the case) the total reflectance $R_{total}(\lambda)$ of a fluorescent sample can be modeled as the ratio of the sum of the purely reflected irradiance $I_0(\lambda)R_{pure}(\lambda)$ of the print, e.g. when illuminated successively by narrow bands $I_0(\lambda)$, and the emitted fluorescent irradiance $F(\lambda)$, when illuminated in the excitation wavelength range, divided by the incident irradiance $I_0(\lambda)$ [85].

$$R_{total}(\lambda) = \frac{F(\lambda) + I_0(\lambda)R_{pure}(\lambda)}{I_0(\lambda)} = \frac{F(\lambda)}{I_0(\lambda)} + R_{pure}(\lambda) \tag{127}$$

Figure 30 shows schematically an example of a fluorescent ink sample of total reflectance R_{total} and pure reflectance R_{pure} printed on a white diffuse support of reflectance R_g. The total reflectance minus the pure reflectance is representative of the fluorescent emission. Obtaining the amount of fluorescent emission is of high interest in many applications, such as the production of paper with fluorescent additives or the analysis of fluorescent probes in biology and medical applications. The pure reflectance can be measured with a double monochromator, one monochromator being used to illuminate the sample and the second one to capture the light emerging from the sample. The pure reflectance of the fluorescent sample is then measured wavelength by wavelength.
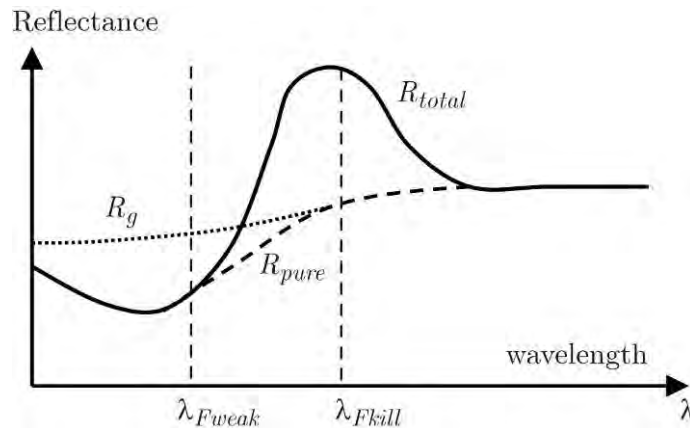

Figure 30. Schematic view of a fluorescent ink sample with total reflectance R_{total} and pure reflectance R_{pure}.

Allen proposed a simple method to obtain the pure reflectance by relying only on a single spectrophotometer and by making three total reflectance measurements, one without filter, one with a fluorescence weakening filter and one with a fluorescence killing filter [83]. Let us call $R_{1tot}(\lambda)$ the total reflectance of the fluorescence sample relative to an illuminant of irradiance $I_1(\lambda)$ and $R_{2tot}(\lambda)$ the total reflectance of the sample relative to the same illuminant attenuated by a fluorescence weakening filter $T(\lambda)$, i.e. relative to an illuminant $T(\lambda)I_1(\lambda)$. The fluorescence

weakening filter has the effect of reducing the fluorescent emission irradiance by a multiplicative factor k. Therefore, according to equation (127) we can express the total reflectance as

$$R_{1tot}(\lambda) = R_{pure}(\lambda) + \frac{F(\lambda)}{I_1(\lambda)} \qquad (128)$$

and

$$R_{2tot}(\lambda) = R_{pure}(\lambda) + \frac{k \cdot F(\lambda)}{T(\lambda)I_1(\lambda)} \qquad (129)$$

With equations (128) and (129) we can express the pure reflectance and eliminate the incident irradiance

$$R_{pure}(\lambda) = \frac{R_{2tot}(\lambda)T(\lambda) - R_{1tot}(\lambda)k}{T(\lambda) - k} \qquad (130)$$

The transmittance $T(\lambda)$ of the fluorescent weakening filter is easily measured with a standard transmittance measurement apparatus. Fluorescent emission intensity factor k can be deduced from the third measurement with a fluorescence killing filter, i.e. a sharp filter blocking the full excitation wavelength range (in Figure 30, blocking all wavelengths lower than λ_{Fkill}). With such a filter, one obtains directly the pure reflectance $R_{pure}(\lambda_{Fkill} < \lambda)$ for wavelengths above λ_{Fkill}.

From equation (130) one may deduce scalar factor k, from a known pure reflectance $R_{pure}(\lambda_{Fkill} < \lambda_\omega)$ at wavelength λ_ω, acquired with a fluorescence killing filter and the total reflectances $R_{1tot}(\lambda = \lambda_\omega)$ and $R_{2tot}(\lambda = \lambda_\omega)$ acquired respectively without filter and with the fluorescence weakening filter

$$k = T(\lambda_\omega)\frac{R_{2tot}(\lambda_\omega) - R_{pure}(\lambda_\omega)}{R_{1tot}(\lambda_\omega) - R_{pure}(\lambda_\omega)} \qquad (131)$$

One should choose a wavelength λ_ω as low as possible, but higher than λ_{Fkill} so to have a sufficiently large difference between the nominator and denominator of equation (131). After having calculated k, equation (130) yields the pure reflectance $R_{pure}(\lambda)$ for all wavelengths of interest, i.e for the wavelengths where $R_{pure}(\lambda)$ and $R_{1tot}(\lambda)$ differ.

9.4. Total reflectances of paper with optical brighteners and of daylight fluorescent inks.

Figure 31 shows the total reflectances of a Canon MP101 paper with fluorescent brighteners (R_p), of the same paper printed with daylight fluorescent yellow (R_y), daylight fluorescent magenta (R_m) and the superposition of the daylight fluorescent yellow and magenta inks (R_{ym}). These total reflectances were measured with a GretagMacbeth Color i7 spectrophotometer, with UV included, i.e. with a light source including UV components between 360 nm and 400 nm.

The fluorescent brighteners located in paper reinforce the blue part of the reflection spectrum of the white patch (Figure 31, R_p). Without them, the paper would look yellowish. The daylight fluorescent inks absorb energy both in the UV wavelength range and in the visible wavelength range. For example, the daylight fluorescent yellow ink absorbs light between 360 and 480 nm and creates a strong fluorescent emission between 500 nm and 575 nm. With a total reflectance of 1.6, the fluorescently emitted light surrounding the 525 nm wavelength is very high and gives the impression of being a light source. The daylight fluorescent magenta ink absorbs in the UV and green wavelength ranges and emits two peaks, one around 440 nm and a second one around 600 nm.

The superposition of the yellow and magenta daylight fluorescent inks shows the interaction between two interacting fluorescent species. The fluorescent emission of the yellow ink is located in the absorption range of the magenta ink and therefore reinforces the fluorescent emission of the magenta ink around 590 nm. This shows that new total reflection spectra can be synthesized by mixing or superposing two or more fluorescent materials.
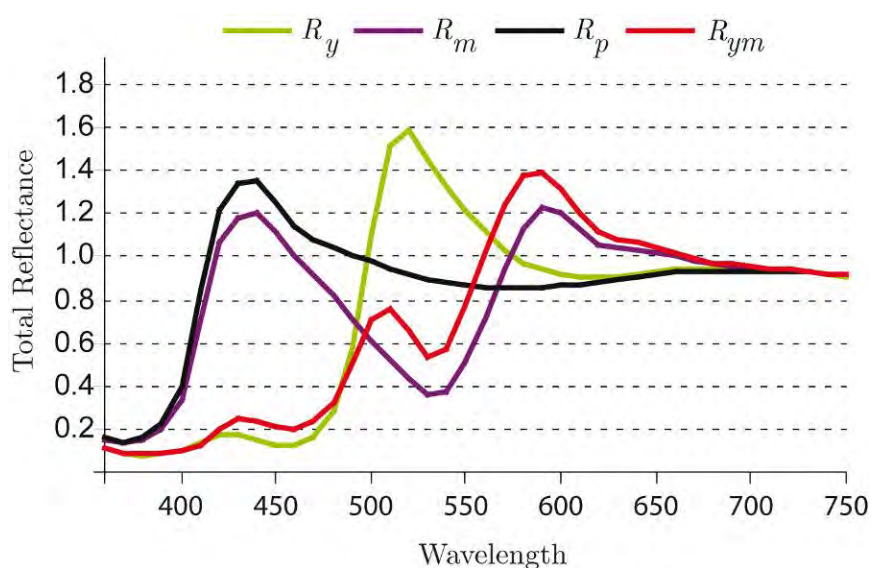

Figure 31. Total reflectances of daylight fluorescent solid inks yellow (R_y), magenta (R_m) and magenta over yellow (R_{ym}) printed on paper with fluorescent brighteners (reflectance R_p).

9.5. Emission spectra of daylight fluorescent inks

Measuring the emission spectra of fluorescent materials, as well as the measurement of any light source requires a carefully calibrated spectrophotometer. Calibration can be performed with a calibrated light source, i.e. a light source having a known relative emission spectrum. From the emission spectrum of the calibrated light source measured by the spectrophotometer, one may derive a wavelength-dependent correction curve. In order to provide correct emission spectra, the intermediate emission spectra values read out from the spectrophotometer need to be multiplied

by this correction curve. Figure 32 shows the normalized emission spectra of the same yellow and magenta daylight fluorescent inks as in Figure 31, but printed on a paper without fluorescent additives. These emission spectra were obtained by illuminating the samples with a Xenon light source, filtered by a U360 UV band pass filter removing all light components above 400 nm.
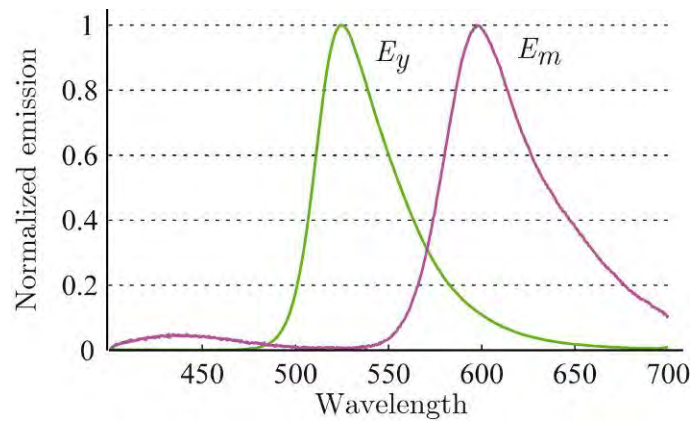

Figure 32. Normalized emission spectra of daylight fluorescent yellow (E_y) and magenta (E_m) solid inks printed on paper without fluorescent brighteners.

9.6. Pure reflectance derived according to Allen's method

Figure 33 shows how the pure reflectance can be deduced from three different measurements of total reflectance. The first total reflectance $R_1(\lambda)$ is obtained by illuminating a yellow fluorescent ink patch with a Xenon light source, the second total reflectance $R_2(\lambda)$ by illuminating the same patch with the same light source but filtered by a fluorescence weakening long pass filter with the transition centered at 450 nm, and the third reflectance $R_3(\lambda)$ by illuminating it with the same light source, filtered by an fluorescence killing long pass filter with the transition centered at 550 nm. Thanks to the fluorescence killing filter, reflectance $R_3(\lambda)$ is the pure reflectance above the cutting edge of the long pass filter and is used to calculate value k at $\lambda_\omega = 575$ nm according to formula (131). The pure reflectance $R_{pure}(\lambda)$ is then calculated according to formula (130).
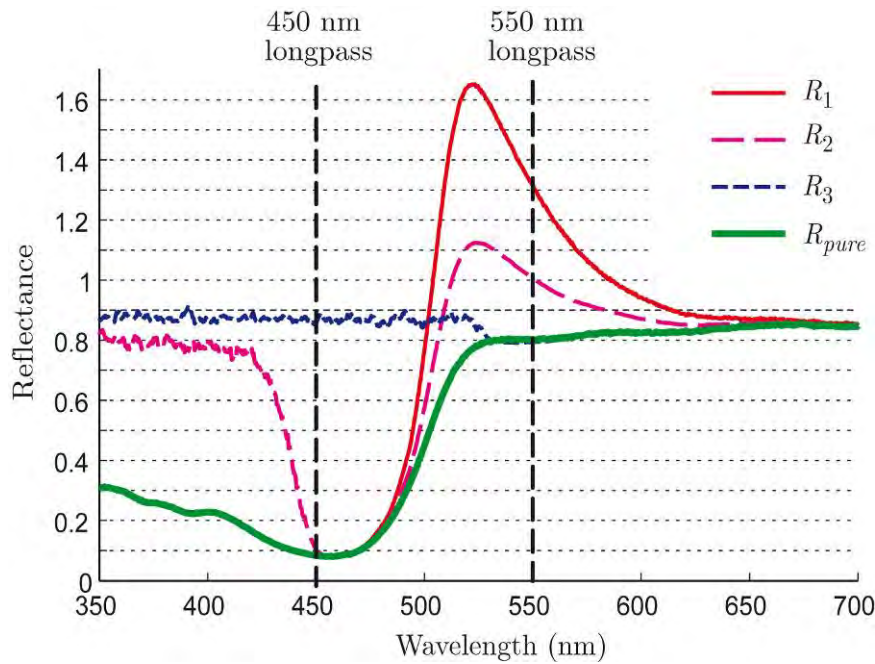
Figure 33. Total reflectance of a daylight fluorescent daylight yellow solid ink printed on a paper without fluorescent additives under a Xenon light source (R_1), total reflectance of the same yellow ink patch under the same illuminant, but filtered by a sharp longpass excitation fluorescent attenuation filter at 450 nm (R_2), reflectance of the same yellow ink patch under the same illuminant filtered by a longpass fluorescence killing filter at 550 nm (R_3) and the resulting pure reflectance spectrum (R_{pure}).

10. CONCLUSIONS

This chapter recaps the key-concepts being at the base of color reproduction models. We insisted on radiometry and light measurement as they two fields are omnipresent in the development and the calibration of surface color rendering models. We also insisted on simple optical phenomena such as absorption, reflexion and refraction by surfaces, by considering different orientations and distributions of the incident light. Regarding scattering, a survey of the main approaches for surface and volume scattering is proposed, in particular le kubelka-Munk model. Fluorescence is also addressed since it is widely used in the papermaking industry in order to give paper a whiter appearance. Throughout this paper, we gave some examples where several basic optical phenomena are composed to form a more complex model. A first example was the slab with flat interfaces, where light undergoes a series of reflexions and refraction by the interfaces and attenuations by absorption (Section 4.2). A second example was the layer of diffusing medium bounded by interfaces with air in reflectance mode or transmittance mode (Sections 7.5 and 7.6). Even more complicated models will be presented in the next chapters for the cases of printed and coated papers or plastics.

APPENDIX A – LAMBERTIAN REFLECTANCE OF INTERFACES

A.1 Relationship between front and back Lambertian reflectances of an interface

The reflectance formula (47) is valid when the Lambertian light comes from the medium with lowest refractive index. When it comes from the other medium, the reflectance is much higher because all rays with incident angle higher than the critical angle $\theta_c = \arcsin(1/n)$ are totally reflected. There exists a simple relation between the two reflectances that we propose here to establish. As previously, we consider media of refractive indices n_1 and $n_2 > n_1$ (the relative index $n = n_2/n_1$ is therefore higher than one). Let us start from the integral expressing the reflectance at the side of medium 2 given by equation (49). We decompose it into two integrals on the intervals $[0, \theta_c]$ and $[\theta_c, \pi/2]$. In the interval $[0, \theta_c]$, relations (30), (37) and (42) yield the equality:

$$R_{21}(\theta_2)\sin 2\theta_2 d\theta_2 = R_{12}(\theta_1)\frac{1}{n^2}\sin 2\theta_1 d\theta_1 \tag{132}$$

Instead of integrating the left member of (132) according to θ_2 on the interval $[0, \theta_c]$, let us integrate the right member according to θ_1 on the corresponding interval $[0, \pi/2]$ in which we retrieve the integral expressing reflectance r_{12} [see equations (46)]:

$$\int_{\theta_2=0}^{\theta_c} R_{21}(\theta_2)\sin 2\theta_2 d\theta_2 = \frac{1}{n^2}\int_{\theta_1=0}^{\pi/2} R_{12}(\theta_1)\sin 2\theta_1 d\theta_1 = \frac{1}{n^2}r_{12} \tag{133}$$

In the interval $[\theta_c, \pi/2]$, the angular reflectance is 1. One therefore has

$$\int_{\theta_c}^{\pi/2} R_2(\theta_2)\sin 2\theta_2 d\theta_2 = \int_{\arcsin(1/n)}^{\pi/2} \sin 2\theta_2 d\theta_2 = 1 - \frac{1}{n^2} \tag{134}$$

The sum of the two integrals provides the relation given in equation (50).

A.2 Numerical values of interface reflectances and transmittances

The reflectances and transmittances of flat interfaces whose numerical values are given in Table B.1 depend only the relative index n. The three reflectances in question, $R_{12}(0)$, r_{12} and r_{21} correspond respectively to the following three illumination geometries: directional illumination at normal incidence, Lambertian illumination from the medium with smallest index, and Lambertian illumination from the other medium. They are respectively given by the equations (33), (47) and (50). The three transmittances $T_{12}(0)$, t_{12} and t_{21}, defined by the same geometries as the reflectances, are simply given by: $T_{12}(0) = 1 - R_{12}(0)$, $t_{12} = 1 - r_{12}$, and $t_{21} = 1 - r_{21}$.

Table B.1. Reflectance and transmittance of interfaces for different relative indices n.

n	$R_{12}(0)$	$T_{12}(0)$	r_{12}	r_{21}	t_{12}	t_{21}
1.30	0.0170	0.9830	0.0611	0.4445	0.9389	0.5555
1.31	0.0180	0.9820	0.0627	0.4538	0.9373	0.5462
1.32	0.0190	0.9810	0.0643	0.4630	0.9357	0.537
1.33	0.0201	0.9799	0.0659	0.4719	0.9341	0.5281
1.34	0.0211	0.9789	0.0675	0.4807	0.9325	0.5193
1.35	0.0222	0.9778	0.0691	0.4892	0.9309	0.5108
1.36	0.0233	0.9767	0.0706	0.4975	0.9294	0.5025
1.37	0.0244	0.9756	0.0722	0.5057	0.9278	0.4943
1.38	0.0255	0.9745	0.0737	0.5136	0.9263	0.4864
1.39	0.0266	0.9734	0.0753	0.5214	0.9247	0.4786
1.40	0.0278	0.9722	0.0768	0.5290	0.9232	0.4710
1.41	0.0289	0.9711	0.0783	0.5364	0.9217	0.4636
1.42	0.0301	0.9699	0.0799	0.5437	0.9201	0.4563
1.43	0.0313	0.9687	0.0814	0.5508	0.9186	0.4492
1.44	0.0325	0.9675	0.0829	0.5577	0.9171	0.4423
1.45	0.0337	0.9663	0.0844	0.5645	0.9156	0.4355
1.46	0.0350	0.965	0.0859	0.5711	0.9141	0.4289
1.47	0.0362	0.9638	0.0873	0.5777	0.9127	0.4223
1.48	0.0375	0.9625	0.0888	0.5840	0.9112	0.4160
1.49	0.0387	0.9613	0.0903	0.5902	0.9097	0.4098
1.50	0.0400	0.9600	0.0918	0.5963	0.9082	0.4037
1.51	0.0413	0.9587	0.0932	0.6023	0.9068	0.3977
1.52	0.0426	0.9574	0.0947	0.6082	0.9053	0.3918
1.53	0.0439	0.9561	0.0962	0.6139	0.9038	0.3861
1.54	0.0452	0.9548	0.0976	0.6195	0.9024	0.3805
1.55	0.0465	0.9535	0.0991	0.6250	0.9009	0.3750
1.56	0.0479	0.9521	0.1005	0.6304	0.8995	0.3696
1.57	0.0492	0.9508	0.1020	0.6357	0.898	0.3643
1.58	0.0505	0.9495	0.1034	0.6408	0.8966	0.3592
1.59	0.0519	0.9481	0.1048	0.6459	0.8952	0.3541

REFERENCES

1   CIE (1987) *International Lighting Vocabulary*; CIE Technical Report, 4th Edition, Publication No 17.4.

2   Born M, Wolf, E. (1999) *Principle of Optics*; Pergamon, Oxford, 7th Edition.

3   Benett, JM (1995) Polarization. *Handbook of Optics Volume I - Fundamentals, techniques and design*; M. Bass (ed). McGraw-Hill, New-York, 2nd Edition.

4   Können, GP. (1985) Polarized light in nature, Cambridge University Press, New-York.

5   Zalewski, EF. (1995) Radiometry and Photometry. *Handbook of Optics Volume II - Devices, measurements and properties (2nd edition)*; Mass M (ed). McGraw-Hill, New-York.

6   Glassner, AS. (1995) *Pinciples of Digital Image Synthesis*; Morgan Kaufmann, San Francisco, Volume 2.

7   McCluney, WR. (1994) *Introduction to Radiometry and Photometry*; Artech House, Boston, MA.

8   Stover, JC. (1995) *Optical scattering, measurement and analysis*, Second Edition, SPIE Optical Engineering Press, Bellingham.

9   Thompson, BJ, Malacara, D. (2001) *Handbook of Optical engineering*; Marcel Dekker, New-York.

10   Wolfe, WL. (1975) *Introduction to Radiometry*; SPIE Optical Engineering Press, Bellingham, WA.

11   Wandlendt, WM, Hecht, G. (1966) *Reflectance spectroscopy*; Interscience Publishers, New-York.

12   Lépine, T, Meyzonnette, JL. (1999) *Bases de radiométrie optique*, Cepadues, Toulouse.

13   Kipphan, H. (2001) *Handbook of Print Media*; Springer Verlag, Berlin.

14   CIE (1998) *Colorimetry*; CIE Technical Report, 3rd Edition.

15   Judd, DB, MacAdam, DL, Wyszecki, G. (1964) Spectral Distribution of Typical Daylight as a Function of Correlated Color Temperature. *Journal of the Optical Society of America* **54**, 1031–1040.

16   CIE (1999) *A Method for Assessing the Quality of Daylight Simulators for Colorimetry*; CIE Technical Report.

17   Nicodemus, FE, Richmond, JC, Hsia, JJ, Ginsberg, IW, Limperis, T. (1977) *Geometrical considerations and nomenclature for reflectance*, NBS Monograph **160**, National Bureau of Standards, Washington, DC, p. 52.

18   Wyszecki, G, Styles, WS. (1982) *Color science: Concepts and methods, quantitative data and formulae*, Wiley, New York, 2nd edition.

19   He, XD, Torrance, KE, Sillion, FX, Greenberg, DP. (1991) A comprensive physical model for light reflection. *Computer Graphics* **25**, 175-186.

20   Borch, J. (1984) *Handbook of physical and mechanical testing of paper and paperboard* (Vol. 2); Mark RE (ed). Marcel Dekker, New York, 1–54.

21   Elias, M, Elias, G. (2004) Radiative transfer in inhomogeneous stratified scattering media with use of the auxiliary function method. *Journal of the Optical Society of America A* **21**, 580–589.

22   Snyder, JP. (1987) *Map Projections – A Working Manual. U. S. Geological Survey Professional Paper 1395*; U. S. Government Printing Office, Washington, DC, 182–190.

23   Judd, DB, Deane, B. (1967) Terms, definitions, and symbols in reflectometry. *Journal of the Optical Society of America* **57**, 445–452.

24   Hébert, M, Hersch, RD, Becker, J-M. (2007) Compositional reflectance and transmittance model for multilayer specimens. *Journal of the Optical Society of America A* **24**, 2628–2644.

25   CIE (1979) *Absolute methods for reflection measurements*; CIE Technical Report.

26   CIE (1986) *Standard standard colorimetric observer*; CIE Technical Report.

27   CIE (1979) *A review of publications on properties and reflection values of material reflection standards*; CIE Technical Report.

28   Simonot, L, Hébert, M, Dupraz, D. (2011) Goniocolorimetry: from measurement to representation in the CIELAB color space. *Color Research and Application* **36**, 169-178.

29   Sharma, G, Vrhel, MJ, Trussell, HJ. (1998) *Color imaging for multimedia.* Proceedings IEEE Transactions on Image processing **86**, 1088–1108.

30   Perkampus, H-H. (1995) *Encyclopedia of Spectroscopy*; VCH, New York.

31   Völz, HG. (2001) *Industrial color testing: Fundamentals and techniques*; Wiley-VCH, New-York, 2nd edition.

32   Kronig, RL. (1926) On the theory of the dispersion of X-rays. *Journal of the Optical Society of America* **12**, 547–557.

33   Miller, A. (1995) Fundamental optical properties of solids. *Handbook of Optics Volume I - Fundamentals, techniques and design*; M. Bass (ed). McGraw-Hill, New-York, 2nd Edition.

34   Orfanidis, SJ. (2010) *Electromagnetic Waves and Antennas*, Rutgers University, p. 27.

35 Malacara, D, Thompson, BJ. (2001) *Handbook of Optical engineering*, Marcel Dekker, New York.

36 Fox, M (2010) *Optical Properties of Solids*, Oxford University Press, New-York, 2nd edition.

37 Hecht, E. (1998) *Optics*, 4rd edition, Addison Wesley.

38 Duntley, SQ. (1942) The Optical Properties of Diffusing Materials, *Journal of the Optical Society of America* **3**, 61–70.

39 Judd, DB. (1942) Fresnel reflection of diffusely incident light. *Journal of the National Bureau of Standards* **29**, 329–332.

40 Heavens, OS. (1997) *Optical Properties of Thin Films*; Dover, New York.

41 Kortüm, G. (1969) *Reflectance Spectroscopy, Principles, Methods, Applications*; Springer-Verlag, Berlin.

42 Torrance, KE, Sparrow, EM. (1967) Theory for Off-Specular Reflection from Roughened Surfaces. *Journal of the Optical Society of America* **57**, 1105–1114.

43 Beckmann, P, Spizzichino, A. (1963) *The scattering of electromagnetic waves from rough surfaces*; Artech House, Norwood, MA, 70–98.

44 Germer, T. (2003) *Polarized light diffusely scattered under smooth and rough interfaces*. Proceedings of SPIE 5158 Polarization Science and Remote Sensing, December 2003. San Jose, CA, 193–204.

45 Cook, RL, Torrance, KE. (1982) A Reflectance Model for Computer Graphics. *ACM Transactions On Graphics* **1**, 7–24.

46 Nayar, SK, Ikeuchi, K, Kanade, T. (1991) Surface reflection: physical and geometrical perspectives. *IEEE Transactions on Pattern Analysis and Machine Intelligence* **13**, 611–634.

47 Elias, M, Menu, M. (2000) Experimental characterization of a random metallic rough surface by spectrophotometric measurements in the visible range, *Optics communications* **180**, 191–198.

48 Elias, M, Menu, M. (2001) Characterization of surface states on patrimonial works of art, *Surface Engineering* **17**, 225–229.

49 Ogilvy, JA. (1991) *Theory of wave scattering from random rough surfaces*, Institute of Physics Publishing, Piladelphia.

50 Stam, J. (2001) An illumination model for a skin layer bounded by rough surfaces. Proceedings 12th Eurographics workshop on Rendering Techniques, June 2001. Springer-Verlag, Berlin, 39–52.

51 Smith, BG. (1967) Geometrical shadowing of a random rough surface, *IEEE Transaction on Antennas and Propagation*, **15**, 668–671.

52 Bruce, NC. (2004) On the validity of the inclusion of geometrical shadowing functions in the multiple-scatter Kirchhoff approximation, *Wave Random Media* **14**, 1–12.

53 Caron, J, Lafait, J, Andraud, C. (2002) Scalar Kirchhoff's model for light scattering from dielectric random rough surfaces. *Optics Communications* **207**, 17–28.

54 Obein, G, Knoblauch, K, Viénot, F. (2004) Difference scaling of gloss: Nonlinearity, binocularity, and constancy. *Journal of Vision* **4**, 711– 720.

55 Obein G, Knoblauch K, Chrisment A, Viénot F. (2002) Perceptual scaling of the gloss of a onedimensional series of painted black samples. *Perception* **31**, p. 65.

56 Hunter, RS, Harold, RW. (1987) *The Measurement of Appearance*; Wiley, Ney-York.

57 Wills, J, Agarwal, S, Kriegman, D, Belongie, S. (2009) Toward a Perceptual Space for Gloss. *ACM Transactions on Graphics* **28**, 103.

58 ASTM (2005) *Standard Termninology of Appearance* (E284-05a); ASTM International.

59 Mie, G. (1908) Beiträge zur Optik trübe Medien, speziell kolloidaler Metallösungen. *Annalen der Physik* **25**, 377–445.

60 Rayleigh, LJS. (1871) On light from the sky, its Polarization and Colour. *Phylosophical Magazine* **41**, 107–120.

61 Prahl, SA. (1988) *Light transport in tissues*. PhD dissertation, University of Texas.

62 Rayleigh, LJS. (1899) On Transmission of Light though an Atmosphere containing Small Particles in Suspension, and on the Origin of the Blue of the Sky. *Phylosophical Magazine*, **47**, 375–384.

63 Henyey, LG, Greenstein, JL. (1941) Diffuse radiation in the galaxy. *Astrophysical Journal* **93**, 70–83.

64 Melamed, NT. (1963) Optical properties of powders: part I. Optical absorption coefficients and the absolute value of the diffuse reflectance. *Journal of Applied Physics* **34**, 560–70.

65 Simonot, L, Hébert, M, Hersch, RD. (2008) Ray scattering model for spherical transparent particles. *Journal of the Optical Society of America A* **25**, 1521–1534.

66 Korringa, J. (1994) Early History of Multiple Scattering Theory for Ordered Systems. *Physics Reports* **238**, 341–360.

67 Chandrasekhar, S. (1960) *Radiative Transfert*; Dover, New-York.

68 Mudgett, PS, Richards, LW. (1971) Multiple scattering calculations for technology. *Applied Optics* **10**, 1485–1502.

69 Klier, K. (1971) Absorption and scattering in plane parallel turbid media. *Journal of the Optical Society of America* **62**, 882–885.

70 Kubelka, P, Munk, F. (1931) Ein Beitrag zur Optik der Farbanstriche. *Zeitschrift für technische Physik* **12**, 593–601.

71 Kubelka, P. (1948) New contributions to the optics of intensely light-scattering material, part I. *Journal of the Optical Society of America A* **38**, 448–457.

72 Maheu, B, Letouzan, JN, Gouesbet, G. (1984) Four-flux models to solve the scattering transfer equation in terms of Lorentz-Mie parameters. *Applied Optics* **23**, 3353–3362.

73 Maheu, B, Gouesbet, G. (1986) Four-flux models to solve the scattering transfer equation: special cases. *Applied Optics* **25**, 1122–1128.

74 Stamnes, K, Tsay, SC, Wiscombe, W, Jayaweera, K. (1988) Numerically stable algorithm for discrete-ordinate-method radiative transfer in multiple scattering and emitting layer media. *Applied Optics* **27**, 2502–2510.

75 Elias, M, Elias, G. (2002) New and fast calculation for incoherent multiple scattering. *Journal of the Optical Society of America A* **19**, 894–905.

76 Van de Hulst, HC. (1980) *Multiple Light Scattering*; Academic Press, New York.

77 Vargas, WE, Niklasson, GA. (1997) Applicability conditions of the Kubelka-Munk theory. *Applied Optics* **36**, 5580–5586.

78 Kubelka, P. (1954) New contributions to the optics of intensely light-scattering materials, part II: Non homogeneous layers. *Journal of the Optical Society of America A* **44**, 330–335.

79 Harris, JW, Stocker, H. (1998) *Handbook of mathematics and computational science*, Springer-Verlag, p. 736.

80 Abramovitz, M, Stegun, IA. (1964) *Handbook of mathematical functions with formulas, graphs, and mathematical tables*, Dover, New-York, p. 1022–1023.

81 Emmel, P. "Physical models for color prediction", *in* Sharma, G, Bala, R. (2003) *Digital Color Imaging Handbook,* CRC Press.

82 Saunderson, JL. (1942) Calculation of the color pigmented plastics. *Journal of the Optical Society of America* **32**, 727–736.

83 Allen E. (1973) "Separation of the spectral radiance factor curve of fluorescent substrates into reflected and fluoresced components," *Applied Optics* **12**, 289–293.

84 Donaldson R. (1954) "Spectrophotometry of fluorescent pigments," *British Journal of Applied Physic* **5**, 210–214.

85 Grum F. (1980) "Colorimetry of Fluorescent Materials," in *Optical Radiation Measurements, Vol. 2, Color Measurements,* (Ed. F. Grum, C.J. Bartelson), Academic Press, New York, 235–288.

86 Rousselle, F, Hébert, M, Hersch, RD. (2010) "Predicting the reflectance of paper dyed with ink mixtures by describing light scattering as a function of ink absorbance" *J. Imaging Science and Technology* **54**, 050501–8.

87 Nobbs J. (1985), "Kubelka—Munk Theory and the Prediction of Reflectance". *Review of Progress in Coloration and Related Topics* **15**, 66–75.

88 Maheu, B, Briton, JP, Gouesbet, G. (1989) "Four-flux model and a Monte Carlo code : comparisons between two simple, complementary tools for multiple scattering calculations." *Applied Optics* **28**, 22–24.

89 Valeur B. (2001) *Molecular Fluorescence*, Chapter 3: Characteristics of fluorescent emission, Wiley-VCH, Weinheim, 34–71.